ESD-TR-72-242

ESD ACCESSION LIST
DRI Call No. 78362
Copy No. 1 of 1 cys.

DRI File Copy

Technical Report 497

An Experimental UHF Ground Surveillance Radar

Volume 2

L. Cartledge
R. D. Yates
Editors

12 October 1972

Prepared for the Department of the Air Force
and the Advanced Research Projects Agency
under Electronic Systems Division Contract F19628-73-C-0002 by

Lincoln Laboratory

MASSACHUSETTS INSTITUTE OF TECHNOLOGY

LEXINGTON, MASSACHUSETTS

ESD RECORD COPY
RETURN TO
SCIENTIFIC & TECHNICAL INFORMATION DIVISION
(DRI), Building 1435

AD757565

Approved for public release; distribution unlimited.

MASSACHUSETTS INSTITUTE OF TECHNOLOGY

LINCOLN LABORATORY

AN EXPERIMENTAL UHF GROUND SURVEILLANCE RADAR
VOLUME 2

L. CARTLEDGE *J. H. TEELE*
M. LABITT *R. D. YATES*

Group 43

TECHNICAL REPORT 497

12 OCTOBER 1972

Approved for public release; distribution unlimited.

LEXINGTON MASSACHUSETTS

The work reported in this document was performed at Lincoln Laboratory, a center for research operated by Massachusetts Institute of Technology. This work was sponsored in part by the Department of the Air Force under Contract F19628-73-C-0002 and in part by the Advanced Research Projects Agency of the Department of Defense under Contract F19628-73-C-0002 (ARPA Order 1559).

This report may be reproduced to satisfy needs of U.S.Government agencies.

Non-Lincoln Recipients

PLEASE DO NOT RETURN

Permission is given to destroy this document when it is no longer needed.

ABSTRACT

This is Volume 2 of the final report summarizing two years of work on ground-based foliage-penetration radar. The design and implementation of a breadboard radar system and of a theoretical and experimental investigation of target and propagation phenomena specific to the foliage-penetration problem are described.

The radar is a coherent UHF system which uses a large (80-foot-diameter), semicircular electronically steered array antenna. All signal processing (including pulse compression), MTI processing, and automatic detection use digital circuitry. The digital signal-processing chain ends in a rather sophisticated thresholding algorithm which provides constant-false-alarm-rate detection for real-time area search operation of the radar. In addition to this area search mode, the radar can be operated as a measurements system which records radar measurements digitally on magnetic tape for more detailed non-real-time processing. Finally, the radar can be operated to produce real-time periodograms of returns from a single range azimuth resolution cell. This mode is useful for monitoring the radar's performance as well as for making preliminary investigations of various target and clutter returns. Operating results and capabilities are described briefly.

Volume 1 comprises three main sections: a short introduction; an overall description of the radar; and detailed descriptions of the hardware and software subsystems in the radar.

Volume 2 describes the use of the radar as a measurements system for studying targets and the clutter environment, in addition to its use for demonstrating the feasibility of radar detection of walking men in foliage. Investigations of target return spectra, clutter return spectra, and clutter return amplitude statistics are reported. Theoretical models relating clutter spectra to wind turbulence and tree resonances are presented and compared with experimental results. Similarly, a previous theoretical prediction of target return spectra is compared with experimental results. Clutter return amplitude statistics are measured and found to be Gaussian under certain conditions. Finally, Vol. 2 contains some comments on the relationships between the subclutter visibility and various parameters of digital MTI systems.

Accepted for the Air Force
Joseph J. Whelan, USAF
Acting Chief, Lincoln Laboratory Liaison Office

CONTENTS

	Abstract	iii
	Acknowledgments	vi
I.	Introduction	1
II.	Clutter Spectrum	2
	A. Theory	2
	B. Experiments	9
	1. Clutter-Model Verification	9
	2. Tree and Wind Experiments	10
	3. Clutter Spectrum Estimates	11
III.	Target Spectrum from Foliated Areas	42
	A. Theory	42
	B. Experiments	46
	1. Transponder Returns	46
	2. Spectrum of Man in Woods	47
	3. Recommendations for Further Work	48
IV.	Clutter Statistics	57
	A. Theory	57
	B. Experiments	59
V.	Subclutter Visibility in Digital MTI Radars	62

ACKNOWLEDGMENTS

In addition to the authors, many other persons made significant contributions to this work. The digital correlator, STC logic, and fast timing were developed by W. Janvrin. The analog receiver was largely designed and packaged by D. S. Rogers. Some of the data presentations were generated by R. Leßlanc. The digital preprocessor was packaged by S. R. Tringale.

Contributors to the programming and implementation of the FDP signal-processing system include J. D. Drinan, A. M. Huntoon, F. Nagy, Jr., W. D. Chapman and R. J. Saliga.

The project received valuable direction from L. W. Bowles, I. Lebow and C. E. Muehe. Administrative and technical help and suggestions were received from H. P. McCabe.

The project would have been impossible without the enthusiastic support of B. Adams, J. Adams, E. Adamczyk, C. Braman, W. Crowder, A. Doiron, A. Gregory, A. L. Lipofsky, R. P. Meuse, C. Repucci and D. Wiggin who worked long and hard, often under demanding conditions.

In addition to the Lincoln Laboratory people listed above, we are indebted to Dr. S. Rosenbaum of Brooklyn Polytechnic Institute for his theoretical contributions, and to Mr. J. Salerno of Harry Diamond Laboratory for suggesting certain experimental techniques.

ANALYSIS AND MEASUREMENTS

I. INTRODUCTION

R. D. Yates

In this Volume, the spectra of clutter and target returns from foliated areas are presented, and a study of the clutter statistics is given. In addition, an expression for the subclutter visibility in digital MTI radars is presented.

The Long Range Demonstration Radar (LRDR) program was terminated on 30 June 1972. The radar as a detection system was debugged and operated satisfactorily by early April. The measurements system part of the radar became operational by the middle of May. Hence, there was a limited time available for science experiments.

In Sec. II, a theoretical model is presented which can predict the clutter spectrum from foliated areas as a function of several parameters. Experiments were conducted which verified the validity of the model. A series of estimated clutter spectra from various areas under different wind conditions is presented.

A theoretical model which can predict the spectrum of a target moving at a constant velocity in foliage is presented in Sec. III. The estimated spectra of a transponder used as a point target, and those of a single man are presented. It appears that the model is valid, but additional tests are outlined to further verify the model.

In Sec. IV, the clutter statistics are considered. Based on theoretical considerations given, it appears that the temporal statistics may be modeled as a Gaussian random process over the time the clutter is statistically stationary. An experiment is presented to verify this model. Additional tests are outlined to study further the spatial and temporal clutter statistics.

Finally, Sec. V presents an expression for the subclutter visibility in digital MTI radars.

II. CLUTTER SPECTRUM

A. Theory

R. D. Yates
M. Labitt

An extensive study has been made of theoretical and experimental models for the clutter power spectral density from wind-blown foliage.[1,2] In this section, the results will be recast in radar terminology and summarized.

Rosenbaum and Bowles[1] model the forest by a flat dielectric slab over a flat conducting ground. The mean or background slab has a refractive index η, an attenuation factor α, and a height h_f. The permittivity of the slab has random fluctuations characterized by the zero mean, complex, space-time random process $\epsilon(\underline{r}, t)$ where $\underline{r} = (x, y, z)$ represents the transverse direction (x, y) and height z, and t is the time. The motion of the scatterers is characterized by a velocity field $\underline{V}(\underline{r}, t)$ which is assumed to be independent of the permittivity process $\epsilon(\underline{r}, t)$. The antenna, which is horizontally polarized, is assumed to be high enough above the forest so that the lateral wave propagation mode can be ignored.

Although general expressions for the clutter power spectral density are derived, the most practical situation is when the forest is assumed to be statistically homogeneous and isotropic in the transverse directions and statistically stationary in time.

Under the above assumptions, and using a range-gated pulse-doppler radar such as the LRDR, the complex envelope of the clutter signal can be expressed as

$$\begin{aligned} X(t) &= I(t) + jQ(t) \\ &= G_r^{1/2} \cdot P_c^{1/2} \cdot C(t) \end{aligned} \tag{II-1}$$

in which $I(t)$ and $Q(t)$ are the in-phase and quadrature components, respectively, and

G_r = receiver gain

P_c = received clutter power per pulse from compressed range cell

$C(t)$ = unit power, complex, clutter random process.

The received clutter power P_c may be written as

$$P_c = P_o \cdot G \cdot A \cdot \sigma_c \cdot F_c \tag{II-2}$$

where

P_o = transmitted peak power

G = one-way antenna gain

A = antenna aperture = $G\lambda^2/4\pi$

σ_c = clutter cross section in m^2

F_c = two-way clutter propagation factor.

Since the forest is assumed to be statistically homogeneous and isotropic in the transverse directions, the clutter cross section σ_c can be expressed in terms of an area cross section σ_o as

$$\sigma_c = \sigma_o \cdot R \cdot \Delta R \cdot \Delta\theta \tag{II-3}$$

where

σ_o = clutter area cross section in m^2/m^2

R = distance to range cell

ΔR = effective range cell length = $cT_p/2$

T_p = effective duration of the compressed pulse

$\Delta\Theta$ = two-way antenna beamwidth.

On letting $P(t)$ denote the compressed pulse, its effective duration is defined as

$$T_p = \frac{\int |P(t)|^2 \, dt}{\max |P(t)|^2} \quad . \tag{II-4}$$

Let the antenna have a one-way gain pattern $P(\Theta, \varphi)$ where Θ and φ are the azimuth and elevation angles, respectively. Since the pattern is chosen so that the elevation beamwidth is large and ground targets are of prime interest, the one-way antenna gain G and two-way beamwidth $\Delta\Theta$ are as follows:

$$G = \max_{\Theta} P(\Theta, 0) = P(0, 0) \tag{II-5}$$

$$\Delta\Theta = \frac{\int_{-\pi}^{\pi} |P(\Theta, 0)|^2 \, d\Theta}{|P(0, 0)|^2} \quad . \tag{II-6}$$

Due to the nature of the clutter model used, it is only possible to express the product $\sigma_o F_c$ in terms of the forest parameters, antenna height, and distance to the range cell as follows:

$$\sigma_o F_c = \frac{\left(\frac{h_a - h_f}{\lambda}\right)^4}{R^8} \cdot \frac{4\pi}{\epsilon_o^2 (\eta^2 - 1)^2} \cdot R(0) \tag{II-7}$$

in which

h_a = antenna height

h_f = slab height

λ = free-space wavelength

R = range to cell

ϵ_o = free-space permittivity

η = slab refractive index.

The function $R(\tau)$ is a correlation function which can be expressed as

$$R(\tau) = \int_o^{h_f} \int_o^{h_f} \varphi\left(\frac{4\pi}{\lambda}; z_1, z_2\right) g(z_1) \, g^*(z_2)$$

$$\times m(z_2, \tau) \exp\left[j \frac{4\pi}{\lambda} \sqrt{\eta^2 - 1} \, (z_1 - z_2)\right] dz_1 \, dz_2 \quad . \tag{II-8}$$

The function g(z) represents the effects of ground lobing and attenuation within the forest and is expressed as

$$g(z) = \exp\left[-a\left(1 - \frac{z}{h_f}\right)\right]\left\{1 - \exp\left[-\frac{z}{h_f}(a + jb)\right]\right\}^2 \tag{II-9}$$

in which

$$a = \frac{2\alpha\eta h_f}{\sqrt{\eta^2 - 1}} \tag{II-10}$$

$$b = \frac{4\pi h_f}{\lambda}\sqrt{\eta^2 - 1} \quad . \tag{II-11}$$

The function $m(z, \tau)$ represents the effects of the motion of the scatterers and is expressed as

$$m(z, \tau) = E\left\{\exp\left[j\,\frac{4\pi}{\lambda}\int_0^{\tau} V_T(z, t)\,dt\right]\right\} \tag{II-12}$$

where $V_T(z, t)$ is the component of the velocity field $\underline{V}(x, y, z, t)$ in the transverse direction (x, y), and E{ } is the statistical expectation operator. If a carrier at (c/λ) Hz is frequency modulated by the random process $(4\pi/\lambda) \cdot V_T(z, t)$, then $m(z, \tau)$ is the correlation function of the modulated signal. It has been assumed that $\underline{V}(\underline{r}, t)$ is statistically stationary with respect to t.

The function $\varphi(k; z_1, z_2)$ represents the spatial spectral density of the random permittivity function $\epsilon(\underline{r}, t)$ with respect to the transverse directions and is expressed as follows:

$$\varphi(\underline{k}; z_1, z_2) = \iint C(\underline{\rho}; z_1, z_2)\exp[-j\underline{\rho} \cdot \underline{k}]\,d^2\underline{\rho}$$

$$= \varphi(|\underline{k}|; z_1, z_2) \text{ due to statistical homogeneity and isotropy in the transverse directions.} \tag{II-13}$$

The function $C(\underline{\rho}; z_1, z_2)$ is the correlation function of the random permittivity and is defined as

$$C(\underline{\rho}; z_1, z_2) = E\{\epsilon(\underline{R}, z_1, t)\,\epsilon^*(\underline{R} - \underline{\rho}, z_2, t)\}$$

$$= C(|\underline{\rho}|; z_1, z_2) \text{ due to statistical homogeneity and isotropy in the transverse directions, and stationarity in time.} \tag{II-14}$$

The clutter process $C(\tau)$ in Eq. (II-1) has a correlation function $R_c(\tau)$ where

$$R_c(\tau) = E\{C(\tau)\,C^*(t - \tau)\}$$

$$= \frac{R(\tau)}{R(0)} \tag{II-15}$$

and where $R(\tau)$ is given by Eq. (II-8). The power spectral density of $C(\tau)$ is denoted as $S_c(f)$ where

$$S_c(f) = \int R_c(\tau)\,e^{-j2\pi f\tau}\,d\tau \quad . \tag{II-16}$$

Due to the way the process C(t) has been defined, it possesses unity power.

Although it is not possible to separate the product $\sigma_o F_c$, three propagation terms contained in Eq. (II-8) are worth noting. If the random fluctuations of the permittivity are ignored, the two-way propagation factor corresponding to a point at height h within the slab is given as

$$F(h) = \frac{1}{(4\pi R^2)^2} \cdot \frac{16\eta^2 (h_a - h_f)^4}{(\eta^2 - 1)^2 \cdot R^4} \cdot |g(h)|^2 \quad . \tag{II-17}$$

The first factor in Eq. (II-17) is the free-space loss, the second is the loss due to the transmission through the slab-free-space interface, and the third is the loss due to ground lobing and attenuation within the slab.

In order to proceed further in evaluating the clutter spectrum, the statistics of the velocity field $\underline{V}(\underline{r}, t)$ and the correlation function of the random permittivity $C(\underline{\rho}; z_1, z_2)$ must be known. However, there are two limiting cases which lead to simple expressions for the correlation function $m(z, \tau)$.

Since the scatterers are bound, the velocity process $V_T(z, t)$ is integrable and a displacement process $D_T(z, t)$ can be defined as

$$D_T(z, t) = \int_o^t V_T(z, s)\, ds + D_T(z, 0) \quad . \tag{II-18}$$

The correlation function $m(z, \tau)$ can then be written as

$$m(z, \tau) = E\left(\exp\left\{j \frac{4\pi}{\lambda} [D_T(z, t) - D_T(z, t - \tau)]\right\}\right) \quad . \tag{II-19}$$

A phase modulation index $\mu(z)$ can then be defined as

$$\mu(z) = \frac{4\pi}{\lambda} \sigma(z) \tag{II-20}$$

$$\sigma^2(z) = \mathrm{Var}\{D_T(z, t)\} \quad . \tag{II-21}$$

The first case of interest is when $\mu(z) \ll 1$. Then, Eq. (II-19) can be approximated as

$$m(z, \tau) = 1 - \mu^2(z) + \mu^2(z) \cdot \rho_D(z, \tau) \tag{II-22}$$

in which $\rho_D(z, \tau)$ is the normalized covariance function of the displacement process and is defined as

$$\rho_D(z, \tau) = E\left\{\frac{D_T(z, t) - \overline{D_T(z, t)}}{\sigma(z)} \cdot \frac{D_T(z, t - \tau) - \overline{D_T(z, t - \tau)}}{\sigma(z)}\right\} \quad . \tag{II-23}$$

In order to derive Eq. (II-22), the statistics of $D_T(z, t)$ need not be known. Only the variance $\sigma^2(z)$ and normalized covariance function $\rho_D(z, \tau)$ are needed.

The second case of interest is when $\mu(z) \gg 1$, and corresponds to the case of large index phase modulation. From Ref. 3, Eq. (II-19) can be approximated as

$$m(z, \tau) = \Psi_v\left(z, \frac{4\pi}{\lambda} \tau\right) \tag{II-24}$$

where $\Psi_v(z, x)$ is the characteristic function of the random process $V_T(z, t)$ and is defined as

$$\Psi_V(z, x) = E\{\exp[jx \cdot V_T(z, t)]\}$$

$$= \int p_V(z, V)\, e^{jxV}\, dV \tag{II-25}$$

where $p_V(z, V)$ is the first-order probability density function of the process $V_T(z, t)$.

There are also simplifications of Eq. (II-8) for the correlation function $R(\tau)$ which result from assumptions about the permittivity process $\epsilon(\underline{r}, t)$. The first case is when it is assumed to be homogeneous with height. Then, the statistics of the velocity field do not depend on height, and the spatial spectrum function $\varphi(k; z_1, z_2)$ is a function of $z_1 - z_2$. Thus, Eq. (II-8) reduces to

$$R(\tau) = R(0)\, m(\tau) \tag{II-26}$$

where

$$R(0) = \int_o^{h_f} \int_o^{h_f} \varphi_1(\tfrac{4\pi}{\lambda}; z_1 - z_2)\, g(z_1)\, g^*(z_2)$$
$$\times \exp\left[j \frac{4\pi}{\lambda} \sqrt{\eta^2 - 1}\, (z_1 - z_2)\right] dz_1\, dz_2 \tag{II-27}$$

$$m(\tau) = E\left(\exp\{j \frac{4\pi}{\lambda} [D_T(t) - D_T(t - \tau)]\}\right) \quad . \tag{II-28}$$

It follows from the above the shape of the clutter spectrum depends only on the statistics of the displacement process $D_T(t)$.

The second, and more important, simplification of Eq. (II-8) is when the spatial spectrum function can be written as follows:

$$\varphi(k; z_1, z_2) = \varphi_2(\tfrac{4\pi}{\lambda}, z_1)\, \delta(z_1 - z_2) \tag{II-29}$$

where $\delta(z)$ is the delta function. Then, Eq. (II-8) can be expressed as

$$R(\tau) = R(0) \cdot \int_o^{h_f} W(z)\, m(z, \tau)\, dz \tag{II-30}$$

in which

$$W(z) = \frac{\varphi_2(\frac{4\pi}{\lambda}, z)\, |g(z)|^2}{\int_o^{h_f} \varphi_2(\frac{4\pi}{\lambda}, z)\, |g(z)|^2\, dz} \tag{II-31}$$

and

$$R(0) = \int_o^{h_f} \varphi_2(\tfrac{4\pi}{\lambda}, z)\, |g(z)|^2\, dz \quad . \tag{II-32}$$

Equation (II-30) would result if one assumed that the scattering was uncorrelated as a function of height and that the effective cross section was proportional to $W(z)$.

Based on heuristic considerations, Labitt[2] was able to choose a weighting function $W(z)$ and a correlation function $m(z, \tau)$ which could model the experimentally measured clutter spectrum fairly well. This model is described below. However, the function $R(0)$ given by Eq. (II-32), which is proportional to the clutter area cross section, could not be determined.

It is assumed that within a range-azimuth cell, all the trees are similar and that their motion may be approximated by a linear dynamic system. The force acting on the trees depends on the velocity of the turbulent wind within the forest. The tree displacement then phase modulates the transmitted carrier frequency.

Let the average wind velocity above the trees be denoted as v_o and the turbulent component within the forest as v(t) which is modeled as a zero-mean, statistically stationary random process. The power spectral density of v(t) may be approximated as[4]

$$S_v(f) = \frac{k}{[1 + (f/f_e)^2]^{5/6}} \tag{II-33}$$

where k is a constant, and f_e is a cutoff frequency. The power of the wind turbulence depends in some manner on the average wind velocity, so that k is a function of v_o. Typical values for the cutoff frequency f_c appear to be 0.01 Hz.

The force acting on the trees will be a nonlinear function of the wind turbulence v(t). Since the trees generally have a highly damped motion, it would seem reasonable to assume that the force F(t) could be expressed as

$$\begin{aligned} F(t) &= [v(t)]^{\nu} \qquad && v(t) > 0 \\ &= -[-v(t)]^{\nu} \qquad && v(t) < 0 \end{aligned} \tag{II-34}$$

where ν is a small positive number. It is also reasonable to assume that v(t) is a Guassian random process. Then the power spectral density of F(t) can be expressed as

$$S_F(f) = \sum_{n=1}^{\infty} A_n S_v^{(n)}(f) \tag{II-35}$$

where $S_v^{(n)}(f)$ is the nth-fold convolution of $S_v(f)$, and A_n are decreasing positive constants. Since $S_v(f)$ is impulsive, except for the exact shape about zero frequency, $S_F(f)$ can be approximated as

$$S_F(f) = \frac{\alpha(v_o)}{[1 + (f/f_1)^2]^{5/6}} \tag{II-36}$$

where f_1 is some convenient cutoff frequency, and $\alpha(v_o)$ determines the dependence of the power in the force F(t) as a function of the average wind velocity.

The tree motion is modeled by a linear dynamic system. In terms of an electrical analog, the force is a voltage source driving a series RLC circuit where the tree displacement is proportional to the charge on the capacitor. The displacement process $D_T(z, t)$ is modeled as

$$D_T(z, t) = \sigma(z) \cdot d(t) \tag{II-37}$$

where $\sigma(z)$ is defined by Eq. (II-21), and d(t) is a normalized displacement process with unity power. It has been assumed that the correlation function of the displacement process depends on the height z only through a gain factor. Since trees bend like a beam, the height dependence of the standard deviation $\sigma(z)$ was taken to be proportional to z^2.

Under the above assumptions, the variance and normalized covariance functions of the displacement process $D_T(z, t)$, which are defined by Eqs. (II-21) and (II-23), respectively, can be written as

$$\sigma^2(z) = \beta^2(v_o) \cdot z^4 \tag{II-38}$$

$$\rho_D(z, \tau) = \rho_d(\tau)$$

$$= \int S_d(f)\, e^{j2\pi f}\, df \tag{II-39}$$

in which $\beta(v_o)$ is a function which depends on the average wind velocity and type of trees and $S_d(f)$ is the power spectral density of the displacement process d(t) and is expressed as

$$S_d(f) = \frac{G_v(f) \cdot G_T(f)}{\int G_v(f) \cdot G_T(f)\, df} \tag{II-40}$$

where

$$G_v(f) = [1 + (f/f_1)^2]^{-5/6} \tag{II-41}$$

$$G_T(f) = \left[1 + \left(2 - \frac{1}{Q_o^2}\right)\left(\frac{f}{f_o}\right)^2 + \left(\frac{f}{f_o}\right)^4\right]^{-1} \quad . \tag{II-42}$$

In Eq. (II-41), f_1 is the cutoff frequency of the wind turbulence; in Eq. (II-42), f_o is the resonant frequency of the trees and Q_o is the "Q" (or quality) factor. Although the limiting form of the correlation function $m(z, \tau)$, given by Eq. (II-22), is now known, for general modulation indices the statistics of d(t) must be known. It was decided to model d(t) as a Gaussian random process so that $m(z, \tau)$ can then be written as

$$m(z, \tau) = \exp\{-\mu^2(z)\,[1 - \rho_d(\tau)]\} \tag{II-43}$$

where $\mu(z)$ is the modulation index, and from Eqs. (II-20) and (II-38) is

$$\mu(z) = \frac{4\pi}{\lambda} \cdot \beta(v_o) \cdot z^2 \quad . \tag{II-44}$$

The normalized covariance function $\rho_d(\tau)$ of the displacement process is given by Eq. (II-39).

The weighting function used in Eq. (II-30) must now be determined in order to obtain an expression for the clutter power spectral density shape. Again, heuristic considerations were used to obtain a reasonable answer.

It was assumed that the density of scatterers as a function of height is given as $\gamma(z)$, and that the field intensity I(z) at height z is the solution of the equation:

$$dI(z) = I(z)\, \gamma(z)\, dz \quad . \tag{II-45}$$

Hence, I(z) can be expressed as

$$I(z) = I(0) \cdot \exp\left[\int_o^z \gamma(h) \cdot dh\right] \quad . \tag{II-46}$$

It follows that the weighting function W(z) can then be expressed as

$$W(z) = \frac{I(z) \cdot \gamma(z)}{I(h_f) - I(0)} \quad . \tag{II-47}$$

Several choices for $\gamma(z)$ were tried and the resulting spectral shapes were compared with the clutter spectra estimated from real data. The best choice of $\gamma(z)$ was found to be $e^{-z^2/2}$. Thus, the weighting function can be written as

$$W(z) = \frac{\exp\{-[L \cdot \operatorname{erfc}(z/\sqrt{2}) + \frac{1}{2} z^2]\}}{\int_0^{h_f} \exp\{-[L \operatorname{erfc}(z/\sqrt{2}) + \frac{1}{2} z^2]\}\, dz} \tag{II-48}$$

in which the parameter L represents the total propagation attenuation within the forest and is given as

$$L = \ln \frac{I(h_f)}{I(0)} \tag{II-49}$$

and erfc(x) is the complementary error function. As a practical matter, h_f was taken to be infinite in Eqs. (II-48) and (II-49).

Using Eqs. (II-39) through (II-44), (II-48) and (II-30), the normalized clutter power spectral density given by Eqs. (II-16) and (II-15) ean be computed. It will be a function of the eutoff frequency of the wind f_1, the resonant frequency of the trees f_o, the "Q" of the trees Q_o, a standard deviation gain factor $\beta(v_o)$ of the displacement proeess which depends on the average wind veloeity v_o and the type of trees, the wavelength λ, and a propagation loss factor L of the forest.

One could question some of the assumptions that were made in order to arrive at an expression for the clutter spectral shape. In the next section, experimental verification of this model will be presented.

B. Experiments

1. Clutter-Model Verification

M. Labitt
R. D. Yates

The clutter model developed in See. A above was tested against data gathered from the Florida Field Site Measurements program. The radar measurement system and cxperiments performed are described in Ref. 5.

The quadrature clutter components from five range cells were recorded simultaneously at 435 and 1305 MHz. The range-azimuth area was flat land with pine trees and light underbrush. The wind velocity above the range-cell loeation was also reeorded.

The clutter speetrum was estimated at UHF and L-band. The tree resonant frequency f_o, tree quality factor Q_o, displacement standard deviation at unit height $\beta(v_o)$, and two-way attenuation L were chosen so that the theoretieal elutter spectrum matched the estimated clutter spectrum at UHF. The frequency was then changed to L-band and the attenuation L chosen so that the theoretical and estimated clutter spectra matched up again.

The displaeement spectrum $S_d(f)$, and the corresponding clutter spectrum $S_c(f)$ at 435 and 1305 MHz, based on the theoretical model, are shown in Fig. II-1. The comparison of the theoretieal and estimated spectra is shown in Figs. II-2 and II-3 for 435 and 1305 MHz, respectively.

The running mean and standard deviation of the wind velocity above the trees are shown in Fig. II-4(a-b) over the time segment used to estimate the clutter spectrum. It is seen that the wind is essentially constant at 10 mph.

The parameters used in the theoretical model are:

	UHF	L-Band
Carrier frequency (MHz)	435	1305
Tree resonant frequency f_o (Hz)	0.375	0.375
Tree quality factor Q_o	3	3
Tree standard deviation at unit height $\beta(v_o)$ (m)	0.021	0.021
Two-way attenuation L (dB)	15	40
Wind cutoff frequency f_c (Hz)	0.01	0.01

Other clutter areas were considered and similar results were obtained. Based on this, it would appear that the clutter model presented in Sec. A can be used to predict the shape of the AC clutter spectrum as a function of the parameters f_c, f_o, Q_o, $\beta(v_o)$, λ and L.

It was not determined whether the exact shape of the clutter spectrum over the range of ±0.1 Hz was predicted correctly. The wind cutoff frequency f_c did not affect the shape of the clutter spectrum outside this region. However, it greatly affects the apparent DC power present. The shape of the scatterer density $\gamma(z)$ about $z = 0$, as given in Eq. (II-45), will affect the amount of DC power present also. When a clutter spectrum was estimated with the DC left in, the difference between the theoretical and estimated DC clutter power was at most 10 dB.

It should be noted that, given a particular range azimuth cell, the observed DC clutter power will be a random variable. For a homogeneous forest, the DC clutter power will be exponentially distributed over the collection of range cells. This makes it difficult to match up the theoretical and estimated clutter spectra near zero frequency.

2. Tree and Wind Experiments

M. Labitt
R. D. Yates

In the clutter model developed in Sec. A, the phase modulation index given by Eq. (II-44) is

$$\mu(z) = \frac{4\pi}{\lambda} \cdot \beta(v_o) \cdot z^2 \quad . \tag{II-50}$$

The function $\beta(v_o)$, where v_o is the average wind velocity above the trees, can be interpreted as the standard deviation of the displacement process $D(z,t)$ at unit height. As v_o increases, the wind turbulence within the trees also increases, so that one could postulate that $\beta(v_o)$ is a monotonically increasing function of v_o. When $\beta(v_o)$ is known, the behavior of the clutter spectrum as a function of v_o can then be determined.

In the clutter model, a displacement process $D(z,t)$ was defined and, based on heuristic arguments, an expression for its power spectrum was given by Eq. (II-40). As seen from Sec. 1 above, the theoretical and estimated clutter spectra could be made to agree. However, the displacement spectrum could only be measured indirectly for low modulation indices.

An experiment designed to check the validity of the displacement spectrum and to estimate the function $\beta(v_o)$ is depicted in Fig. II-5. A thin horizontal wire was attached to a tree trunk 3 m above the ground, looped over a stationary pulley, and attached to a small weight. The pulley shaft was connected to a precision servo potentiometer. A DC voltage was applied to the potentiometer, the output of which was connected to an A/D converter. A hot wire anemometer was used to measure the wind speed at the treetop level in the area of the tree. Its output was also connected to an A/D converter. The digitized data were recorded on magnetic tape in the same manner as for the clutter and target data.

The power spectral density estimate of the wind velocity is given in Fig. II-6. As expected, an $f^{-5/3}$ roll-off in frequency was observed.

The power spectral density estimate of the tree displacement is given in Fig. II-7. In addition, the theoretical displacement spectrum given by Eq. (II-40) is shown.

In estimating the displacement spectrum, the DC eomponent was removed, hence, the notch at zero frequency. It is seen that the estimated displacement spectrum is wider about ±0.1 Hz than the theoretical spectrum. There are also two spikes present at ±0.9 Hz.

With the anemometer 30 m from the tree, the squared coherency function between the wind velocity and tree displacement was estimated, as shown in Fig. II-8. One would expeet no correlation between the tree displacement and wind velocity. It is seen that a correlation exists at ±0.9 Hz and about zero frequency. Based on these results, it was dedueed that the spectral broadening about 0 Hz in the displaeement spectrum was due to system instabilities. The lines at ±0.9 Hz were due to a resonance in the measurement system, possibly in the wire or potentiometer.

Based on the abovc results, one can conclude that the theoretical expression for the displaeement spectrum is accurate.

The next problem considered was the behavior of the funetion $\beta(v_o)$. Due to the fact that the displacement spectrum has most of its power near zero frequency, a measurement of its standard deviation would be dominated by low-frequency components. The displacement process model assumed that the displacement spectrum shape was independent of the average wind speed. It follows that the variance of the derivative of the displacement process can be expressed as

$$\sigma_{\dot{D}}^2 = \beta^2(v_o) \cdot z^4 \cdot |\ddot{\rho}_D(o)| \qquad \text{(II-51)}$$

where $\ddot{\rho}_D(o)$ is the second derivative of the normalized displacement covariance function. It follows that the behavior of $\beta(v_o)$ ean also be determined from $\sigma_{\dot{D}}$.

The tree displacement samples and corresponding wind velocity samples were divided into eonseeutive bloeks of 6 minutes in duration. The sample mean $\hat{v}_o$ of the wind, and sample variance $\hat{\sigma}_{\dot{D}}^2$ of the tree velocity were computed for each block. The plot of $\hat{\sigma}_{\dot{D}}^2$ vs $\hat{v}_o$ is shown in Fig. II-9. A least-mean-squarc-error fit of $\sigma_{\dot{D}} = a \cdot v_o^b$ indicated that b = 1.47, with a correlation coefficient of 0.937. The estimate of the variance of the tree velocity was computed by taking discrete Fourier transforms over the block, multiplying the magnitude squared of the frequency coefficients by f^2, and summing all the modified coeffieients.

Based on these results, it is postulated that the function $\beta(v_o)$ has the following form:

$$\beta(v_o) = K \cdot v_o^{1.5} \qquad \text{(II-52)}$$

where K depends on the type of forest.

It should be remarked that Eq. (II-52) was deduced for wind speeds between 0 and 20 mph. It is not clear if this expression is valid well beyond 20 mph.

3. Clutter Speetrum Estimates

The measurement mode of the LRDR was used to record the quadrature components of the elutter return from five eonsecutive range cells from three foliage areas under different wind conditions. The wind velocity at the top of the antenna tower was also recorded.

(a) Spectral Estimation Scheme

M. Labitt
R. D. Yates

A detailed discussion of clutter and target returns and the estimation of their power spectral density is given in Ref. 5. A summary of the estimation scheme is presented here for completeness.

In the LRDR, the compressed, range-gated, quadrature video signal samples are produced at a rate of $(555.6 \times 10^{-6})^{-1} = 1799.8560$ Hz per channel. The TAPWRITE program reduces the data rate to 112.4910 Hz by segmenting the data into consecutive blocks, each block containing 16 points. These points are added together to form one new data point. The quadrature components from five consecutive range cells are then recorded on digital magnetic tape.

A series of computer programs, written to analyze the data from the Florida Everglades measurement program, was used to study the data produced by the LRDR measurement program. The basic procedure may be divided into three steps.

The first step is to filter the data further, depending on the frequency extent of the signals being studied. The data per quadrature channel were divided into consecutive groups of N_a points per group. The N_a points in each group were then added to produce one filtered data point. The sampling rate of the filtered data is then

$$f_s = \frac{112.4910}{N_a} \text{ Hz} \quad . \tag{II-53}$$

The second step consists of forming a set of frequency coefficients using the FFT (fast Fourier transform) algorithm. The data per quadrature channel are divided into B consecutive blocks, each block containing N points. Let $\left\{I_n^{(b)}, Q_n^{(b)}\right\}_{n=0}^{N-1}$ be the N samples of the in-phase and quadrature components of the bth block. Let the complex signal sample $X_n^{(b)}$ be defined as

$$X_n^{(b)} = I_n^{(b)} + jQ_n^{(b)} \quad . \tag{II-54}$$

The N frequency coefficients $\left\{A_k^{(b)}\right\}_{k=0}^{N-1}$ for the bth block are computed as

$$A_k^{(b)} = \sum_{n=0}^{N-1} X_n^{(b)} \cdot W_n \exp\left[-j \frac{2\pi}{N} nk\right] \tag{II-55}$$

in which $\{W_n\}$ are a set of time weights used to obtain the appropriate frequency resolution. In all cases, they were chosen as

$$W_n = \left(\frac{8}{3Nf_s}\right)^{1/2} \cdot \sin^2 \frac{\pi}{N}\left(n + \frac{1}{2}\right) \quad . \tag{II-56}$$

In Eq. (II-55), N was constrained to be a power of 2. The spectral estimates, based on one FFT, are then defined as

$$P_k^{(b)} = \left|A_k^{(b)}\right|^2 \tag{II-57}$$

The third step is to smooth the estimates given by Eq. (II-57) using the data from the B blocks. The N smoothed estimates, $\left\{P_k\right\}_{k=0}^{N-1}$, were computed as

$$P_k = \frac{1}{B} \sum_{b=1}^{B} P_k^{(b)} \quad . \tag{II-58}$$

The samples $X_n^{(b)}$ in Eq. (II-55) can be interpreted as a continuous signal X(t) sampled every $1/f_s$ sec. Hence,

$$X_n^{(b)} = X\left[(n + bN)\ \frac{1}{f_s}\right] \quad . \tag{II-59}$$

On assuming that the signal X(t) is a stationary random process with a power spectral density $S_x(f)$, and that the sampling is high enough so that no aliasing takes place, the estimates of the spectrum $S_x(f)$ are then taken as

$$\hat{S}_x\left(\frac{kf_s}{N}\right) = \begin{cases} P_k & \text{for } k = 0, 1, 2, \ldots, \frac{N}{2} \\ P_{N-k} & \text{for } k = -1, -2, \ldots, -\frac{N-2}{2} \end{cases} \quad . \tag{II-60}$$

The expected value of P_k can be shown to be

$$E\{P_k\} = \int_{-(f_s/2)}^{f_s/2} \tilde{S}_x(f)\ R\left(\frac{kf_s}{N} - f\right)\ df \tag{II-61}$$

in which R(f) is a frequency resolution function, and $\tilde{S}_x(f)$ is the aliased version of $S_x(f)$.

The resolution function R(f) is given in terms of the time weights $\{W_n\}$ as

$$R(f) = \left| \sum_{n=0}^{N-1} W_n \exp\left[-j\ \frac{2\pi nf}{f_s}\right] \right|^2 \quad . \tag{II-62}$$

The aliased spectrum $\tilde{S}_x(f)$ is expressed in terms of $S_x(f)$ as

$$\tilde{S}_x(f) = \sum_{m=-\infty}^{\infty} S_x(f - mf_s) \quad . \tag{II-63}$$

On assuming that the spectral estimates from block-to-block are uncorrelated, the variance of P_k is given as

$$\mathrm{Var}\{P_k\} = \frac{\mathrm{Var}\{P_k^{(b)}\}}{B} \quad . \tag{II-64}$$

The right-hand side of Eq. (II-64) does not depend on b due to the assumption that X(t) is statistically stationary. If X(t) is a Gaussian process, then $\mathrm{Var}\{P_k^{(b)}\} = E^2\{P_k^{(b)}\}$, so that

$$\frac{\mathrm{Var}\{P_k\}}{E^2\{P_k\}} = \frac{1}{B} \quad . \tag{II-65}$$

The spectral estimate of a random process based on one FFT is seen to have a variance governed by Eq. (II-64) with B = 1. Hence, in order to obtain a reliable estimate, B should be large. It was found that adequate estimates of the clutter spectrum could be obtained with B in the range of 50 to 100.

The resolution of the estimates is governed by the choice of $\{W_n\}$. The equivalent rectangular bandwidth of R(f), over its main period $|f| \leqslant f_s/2$, is defined as

$$f_r = \frac{\int_{-(f_s/2)}^{f_s/2} R(f)\, df}{\max\limits_{|f| \leqslant (f_s/2)} R(f)} \quad . \tag{II-66}$$

On letting the weights $\{W_n\}$ be real, and normalizing R(f) so it has unit area over its main period, it follows that

$$\int_{-(f_s/2)}^{f_s/2} R(f)\, df = 1 \tag{II-67}$$

$$R(-f) = R(f) \tag{II-68}$$

$$\max_{|f| \leqslant (f_s/2)} R(f) = R(0) = \frac{1}{f_r} \quad . \tag{II-69}$$

On using the weights given by Eq. (II-56), it follows that the equivalent rectangular bandwidth is given as

$$f_r = \frac{3 \cdot f_s}{2N} \quad . \tag{II-70}$$

The resolution function has zeros at $f = \pm k f_s/N$ for $k = 2, 3, \ldots, N/2$, and the maximum of the sidelobes occurs approximately at

$$f = \pm \frac{(k + \frac{1}{2})\, f_s}{N}$$

for $k = 2, 3, \ldots, (N-2)/2$. The first 6 sidelobes are 31.5, 41.5, 48.5, 54, 58, and 62 dB below the main peak. The value of R(f) at $\pm f_s/N$ is 6 dB below the main peak. The equivalent rectangular bandwidth f_r can be used as a measure of the resolution of the spectral estimates.

Given that R(f) possesses adequate resolution, it follows that Eq. (II-61) can be approximated as

$$E\{P_k\} = P_{DC} \cdot R\left(\frac{kf_s}{N}\right) + S_{AC}\left(\frac{kf_s}{N}\right) \tag{II-71}$$

where it has been assumed that

$$S_x(f) = P_{DC}\delta(f) + S_{AC}(f) \quad . \tag{II-72}$$

Hence, if the spectrum of X(t) has a DC component, it will only appear in the estimates P_0, P_1, P_{-1}.

In practice, the statistics of the process X(t) may not be stationary across the B blocks used to compute the spectral estimates. In the case of clutter, when the phase modulation index is less than 1, it follows from Sec. II-A that the AC clutter spectrum shape does not vary as a function of the average wind velocity. However, the AC clutter power does. By estimating the AC power in each block, and normalizing the data to unit AC power, the smoothing from block-to-block should be more efficient. The sample mean M_b and sample variance S_b^2, for the bth block, were computed as follows:

$$M_b = \frac{1}{N} \sum_{n=0}^{N-1} X_n^{(b)} \tag{II-73}$$

$$S_b^2 = \frac{1}{N-1} \sum_{n=0}^{N-1} |X_n^{(b)} - M_b|^2 \quad . \tag{II-74}$$

The normalized data from the bth block were then taken as

$$\tilde{X}_n^{(b)} = \frac{X_n^{(b)} - M_b}{S_b} \quad . \tag{II-75}$$

The spectral estimates based on the normalized samples are then computed.

It was also of interest to estimate the cross correlation between different signals. Let the two stationary random processes X(t) and Y(t) have power spectra $S_x(f)$ and $S_y(f)$ and a cross spectrum $S_{xy}(f)$. The function of interest is the squared coherency function defined as

$$C_{xy}(f) = \frac{|S_{xy}(f)|^2}{S_x(f) \cdot S_y(f)} \quad . \tag{II-76}$$

The cross spectrum $S_{xy}(f)$ is defined as the Fourier transform of the cross-correlation function $R_{xy}(\tau) = E\{X(t)\, Y^*(t-\tau)\}$. If there is no correlation between X(t) and Y(t), then $C_{xy}(f) = 0$. On the other hand, complete correlation leads to $C_{xy}(f) = 1$. It has been assumed that X(t) and Y(t) contain no specular components so that no impulses are present in the spectra.

The squared coherency function was estimated by assuming the spectra of X(t) and Y(t) as already described, and the cross spectra by replacing $|A_k^{(b)}|^2$ in Eq. (II-57) by $A_{x,k}^{(b)} \cdot A_{y,k}^{(b)*}$, where * denotes the complex conjugate operation, $A_{x,k}^{(b)}$ the frequency coefficients of the process X(t), and $A_{y,k}^{(b)}$ those of Y(t). The estimate of the squared coherency function was then taken as

$$\hat{C}_{xy}(f_k) = \frac{|\hat{S}_{xy}(f_k)|^2}{\hat{S}_x(f_k) \cdot \hat{S}_y(f_k)} \quad . \tag{II-77}$$

On assuming adequate resolution and the absence of specular components, it can be shown that

$$E\{\hat{C}_{xy}(f_k)\} = C_{xy}(f_k) + \frac{1}{B} \tag{II-78}$$

$$\mathrm{Var}\{\hat{C}_{xy}(f_k)\} = \frac{2}{B}\,[C_{xy}(f_k) + C_{xy}^2(f_k)] + \frac{1}{B^2} \tag{II-79}$$

where

$$f_k = \frac{k f_s}{N} \quad . \tag{II-80}$$

The estimation schemes described were extensively tested against both real and simulated data. It was found that the power spectral densities and coherency functions could adequately be estimated by the methods described in this section.

The estimated clutter spectra and squared coherency functions are shown in Figs. II-10 through II-29. Three areas were considered, each one consisting of five consecutive range cells. The range cells were 15 m in length and the azimuth beamwidth was 2.5°. The parameters of range-cell areas studied are given in Table II-1.

TABLE II-1
PARAMETERS OF RANGE-CELL AREAS STUDIED

	Area 1	Area 2	Area 2	Area 3	Area 3
First range-cell number	313	413	413	1120	1120
Beam number	26	5	5	26	26
Range to first cell (km)	5.7	7.2	7.2	17.8	17.8
Approximate wind speed at antenna tower (mph)	5 to 10	10 to 20	10 to 20	5 to 10	10 to 20
Tape number	28	31	31	29	22
Records analyzed	1006 to 2005	401 to 800	11 to 400	6 to 2400	6 to 2005
30-dB bandwidth of clutter spectra (Hz)	±1.43	±2.81	±3.84	±1.48	±2.25
Figure numbers	II-10 to -16	II-17 to -19	II-20 to -22	II-23 to -26	II-27 to -29

The estimates of the clutter power spectrum for each range cell are presented on a decibel vs frequency, and a decibel vs log-frequency scale. The latter case is useful in determining the slope of the clutter spectrum tails. The average of the spectra of the five range cells is also given. The squared coherency function between selected range cells is given to determine if any correlation exists. If there were antenna motion for example, the DC clutter in each range cell would be modulated in an identical manner. This common signal would then appear in the coherency function.

In most tests, the wind speed at the top of the antenna tower was recorded. The running mean and standard deviation of the wind speed for the time duration of the data used to estimate the spectra are presented. Since the range cells were at least 5.7 km from the radar, the wind speed at the range-cell location could be different. If the clutter spectrum bandwidth is to be correlated with the wind velocity, a wind sensor should be placed at the range-cell location.

Area 1 was 5.7 km from the radar. The clutter spectral estimates, with the DC filtered out before the estimation was made, are shown in Figs. II-10 through II-13; Figs. II-14 through II-16 show the estimated spectra of the same data with the DC left in.

It is seen that the spectra have the shape predicted by the clutter model presented in Sec. II-A-1. The resonant frequency of the trees is seen to be 0.336 Hz. With the DC removed, it appears that the shape of the spectra in the region ±0.140 Hz is identical to the turbulent wind velocity spectra. The tails of the clutter spectra have a slope slightly less than $-5\frac{2}{3}$ in cells 1 through 4. In cell 5, the slope is $-5\frac{2}{3}$. The flat section of the spectra past ±3 Hz is due to the receiver noise. It is seen that the DC clutter power from cell-to-cell in Figs. II-14(b) through (f) is not constant. The width of the spectra 30 dB below the tree resonant peaks is ±1.43 Hz.

System tests indicated that the DC offsets in the quadrature video channels were negligible. Hence, the DC powers shown are entirely due to the clutter signal. When comparing the DC-to-AC power, it should be remembered that the estimated DC power at 0 Hz is equal to $K \cdot P_{DC} \cdot f_r^{-1}$, where K is a system constant, P_{DC} is the DC clutter power, and f_r is the frequency resolution. The AC spectrum is equal to $K \cdot S_{AC}(f)$, where $S_{AC}(f)$ is the AC clutter spectrum, when adequate resolution exists. Tests were made to ensure that adequate resolution was used in all the spectral estimates presented.

The squared coherency function between several range-cell pairs is shown in Figs. II-12(a) through (e) with the DC absent, and in Figs. II-16(a) through (e) with DC present. If no correlation exists between range cells, then the mean and standard deviation of the estimate of the squared coherency function are B^{-1}, where B is the number of data blocks used to smooth the estimates. It is seen that no correlation exists between nonadjacent range cells. There is partial correlation between adjacent cells, as seen in Figs. II-12(a) and (e), due to the fact that the basic 100-nsec pulse is passed through a 10-MHz filter at the receiver which causes the apparent range-cell length to be wider than 15 m.

Area 2 was 7.2 km from the radar. Spectral estimates for two different wind conditions are shown in Figs. II-17 through II-19 and II-20 through II-22, respectively. The frequency resolution used is identical in both cases. However, due to the extent of the spectrum, the tree resonant frequency could not be resolved.

In the first case, the 30-dB bandwidth is ±2.81 Hz, while for the second, it is ±3.84 Hz. These were the widest clutter spectra seen thus far. Comparing corresponding range cells in both cases, it is seen that as the AC clutter spectrum spreads out, the DC power is reduced. Again, this was predicted by the clutter model.

Area 3 was 18 km from the radar. Spectral estimates for two different wind conditions are shown in Figs. II-23 through II-26 and II-27 through II-29, respectively. The first case is for a low wind velocity. The clutter spectrum has the shape as predicted by the clutter model. The tree resonant frequency in this case is 0.3 Hz. The slope of the clutter spectrum tails is seen to be approximately $-5\frac{2}{3}$. There is no correlation between nonadjacent range cells. The 30-dB bandwidth is seen to be ±1.48 Hz. Within the experimental error, this is the same as the bandwidth for the clutter spectra from area 1.

The second case is for a higher wind velocity. The 30-dB bandwidth has increased to ±2.25. Comparing corresponding range cells for the two cases, it is seen that as the AC clutter spectrum spreads out, the DC clutter power is reduced. Again, there is no correlation between nonadjacent range cells.

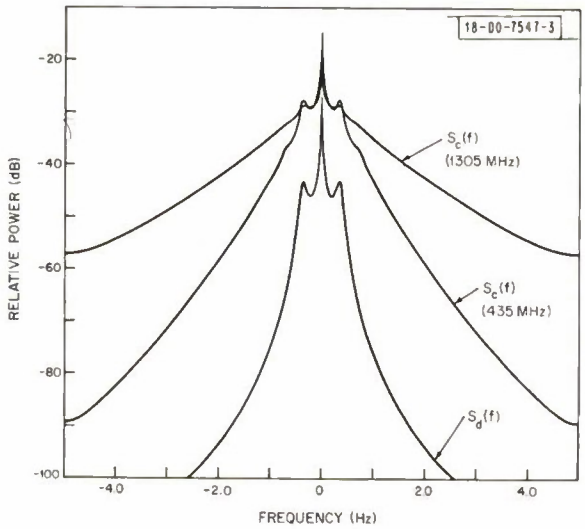

Fig. II-1. Theoretically computed displacement spectrum $S_d(f)$, and clutter spectra $S_c(f)$.

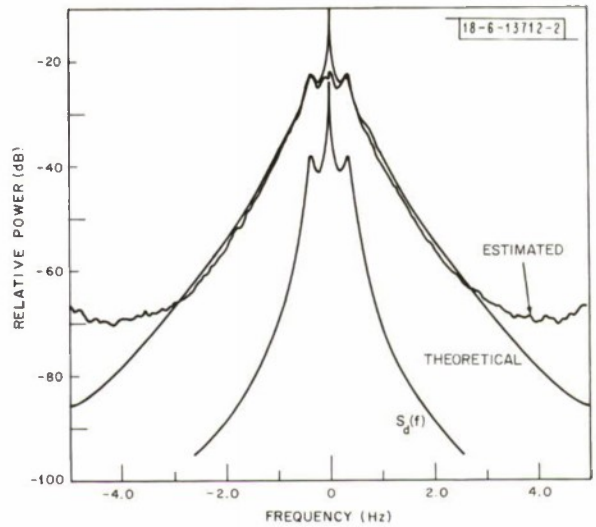

Fig. II-2. Comparison between theoretical and estimated clutter spectra at 435 MHz.

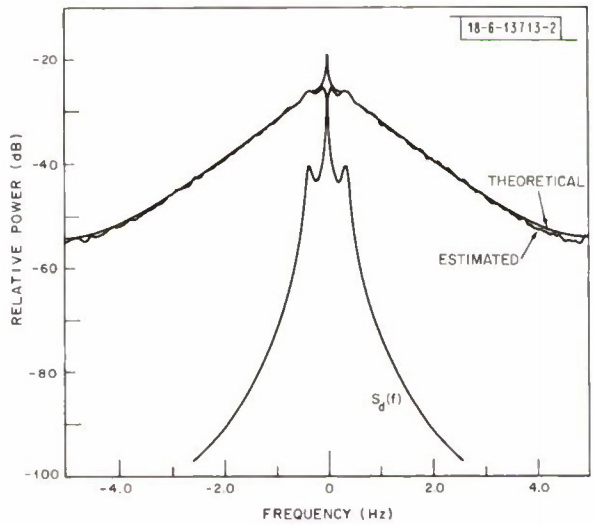

Fig. II-3. Comparison between theoretical and estimated clutter spectra at 1305 MHz.

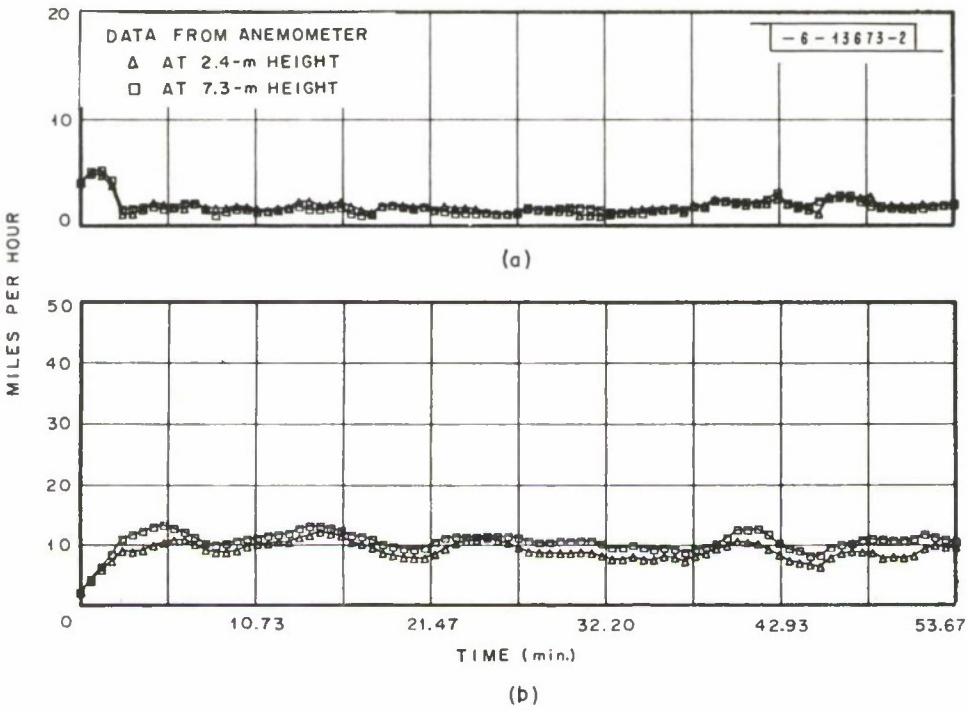

Fig. II-4. Wind data for clutter tape: (a) running standard deviation of wind; (b) running average of wind.

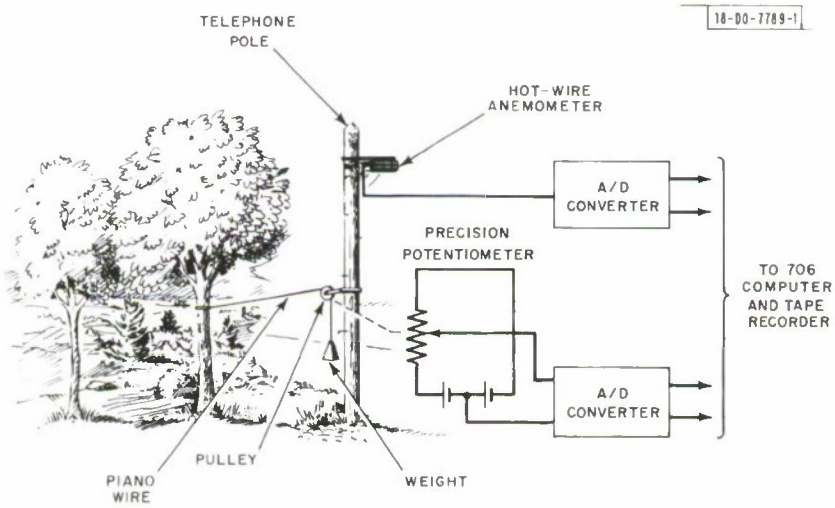

Fig. II-5. Wind and tree motion instrumentation.

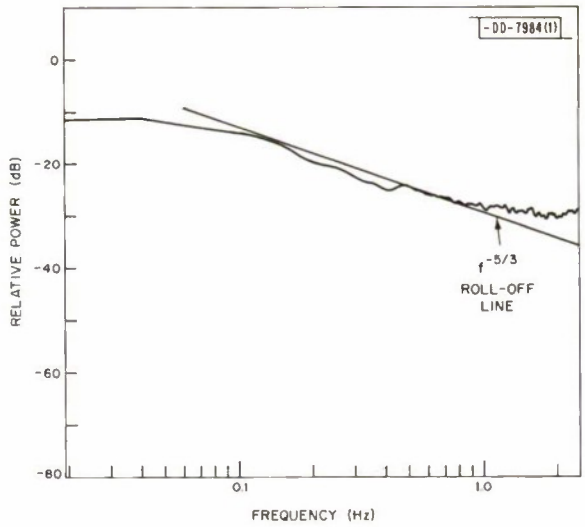

Fig. II-6. Wind spectral estimation. A hot wire anemometer was used as sensor. As expected, curve approximates an $f^{-5/3}$ roll-off observed by many other experimenters.

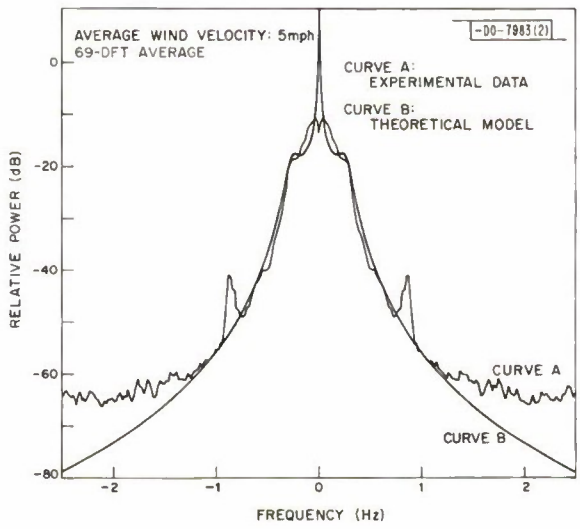

Fig. II-7. Tree displacement spectrum. Spikes at ±0.9 Hz are spurious. Leveling off at −65 dB caused by system noise. Notch at 0 Hz because algorithm removes DC.

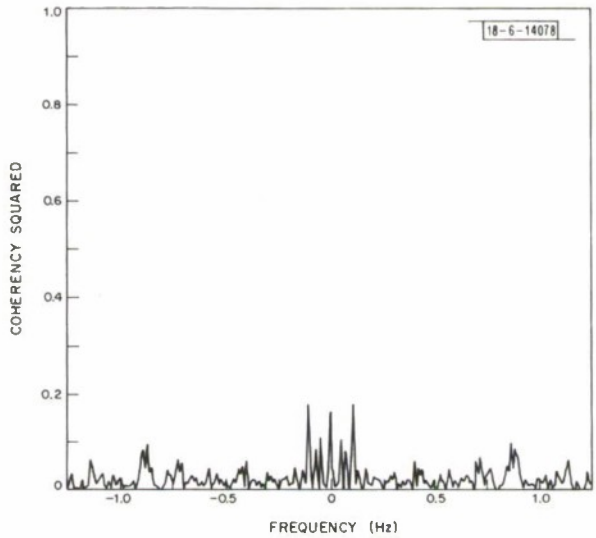

Fig. II-8. Squared coherency spectral estimation between wind and tree displacement. Here, wind and tree sensors were more than 30 m apart. One would not expect any correlation, but some is observed near 0 and 0.9 Hz; these are believed to be spurious.

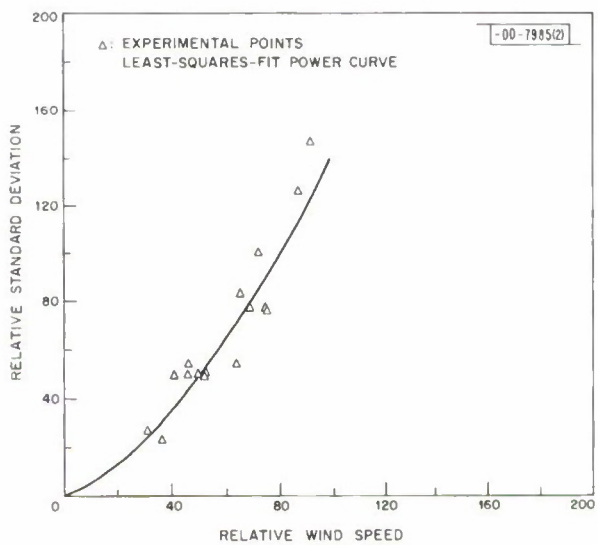

Fig. II-9. Estimated standard deviation of tree velocity vs estimated wind speed. Superimposed is a least-mean-square-error power-law fit. $\sigma_{\dot{D}} = a \cdot v_o^{1.47}$.

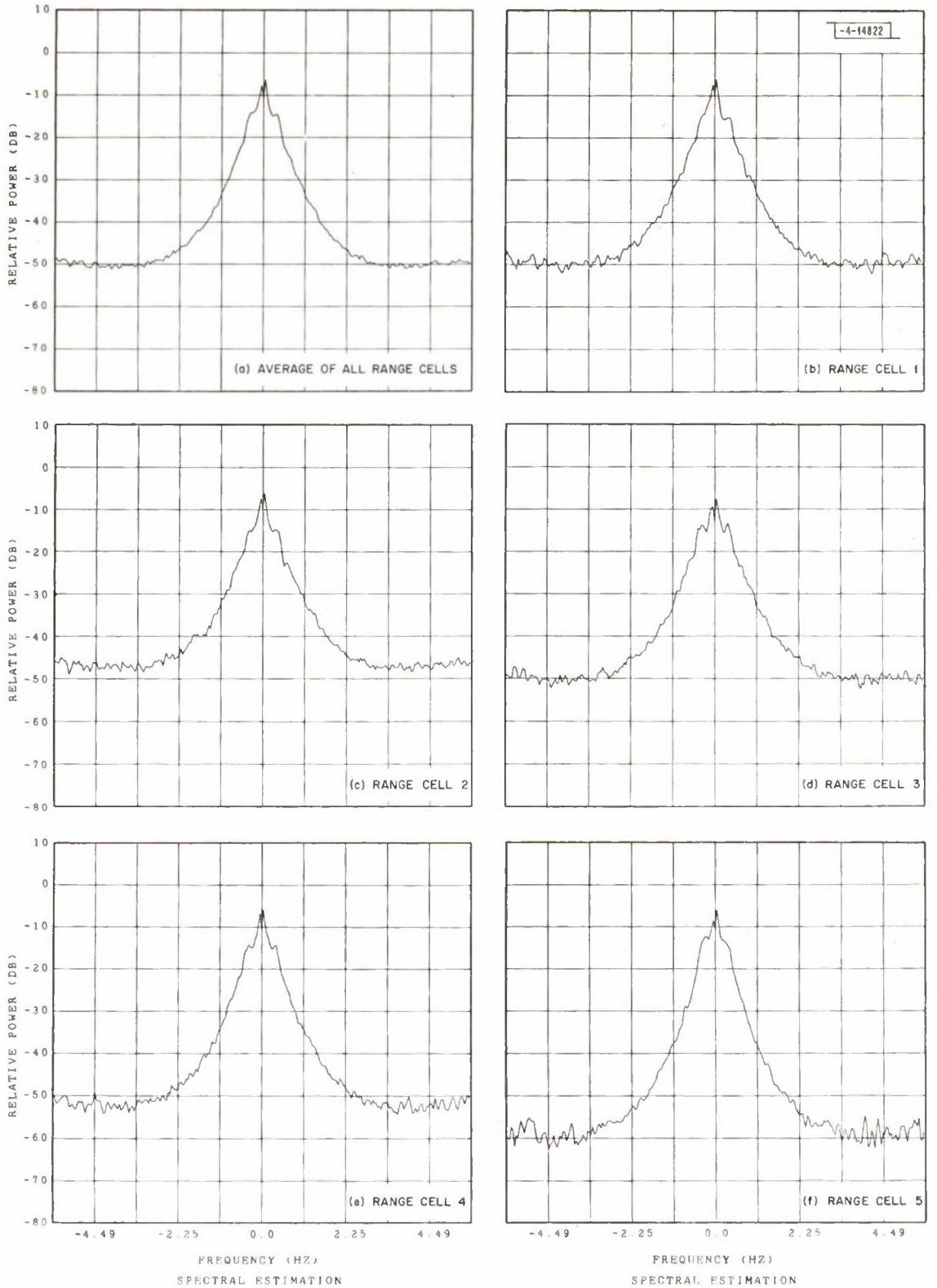

Fig. II-10. Clutter from area 1. DFT length = 256, resolution = 0.0659 Hz, sampling rate = 11.25 Hz. (a) DFTs averaged = 270; (b) through (f) DFTs averaged = 54.

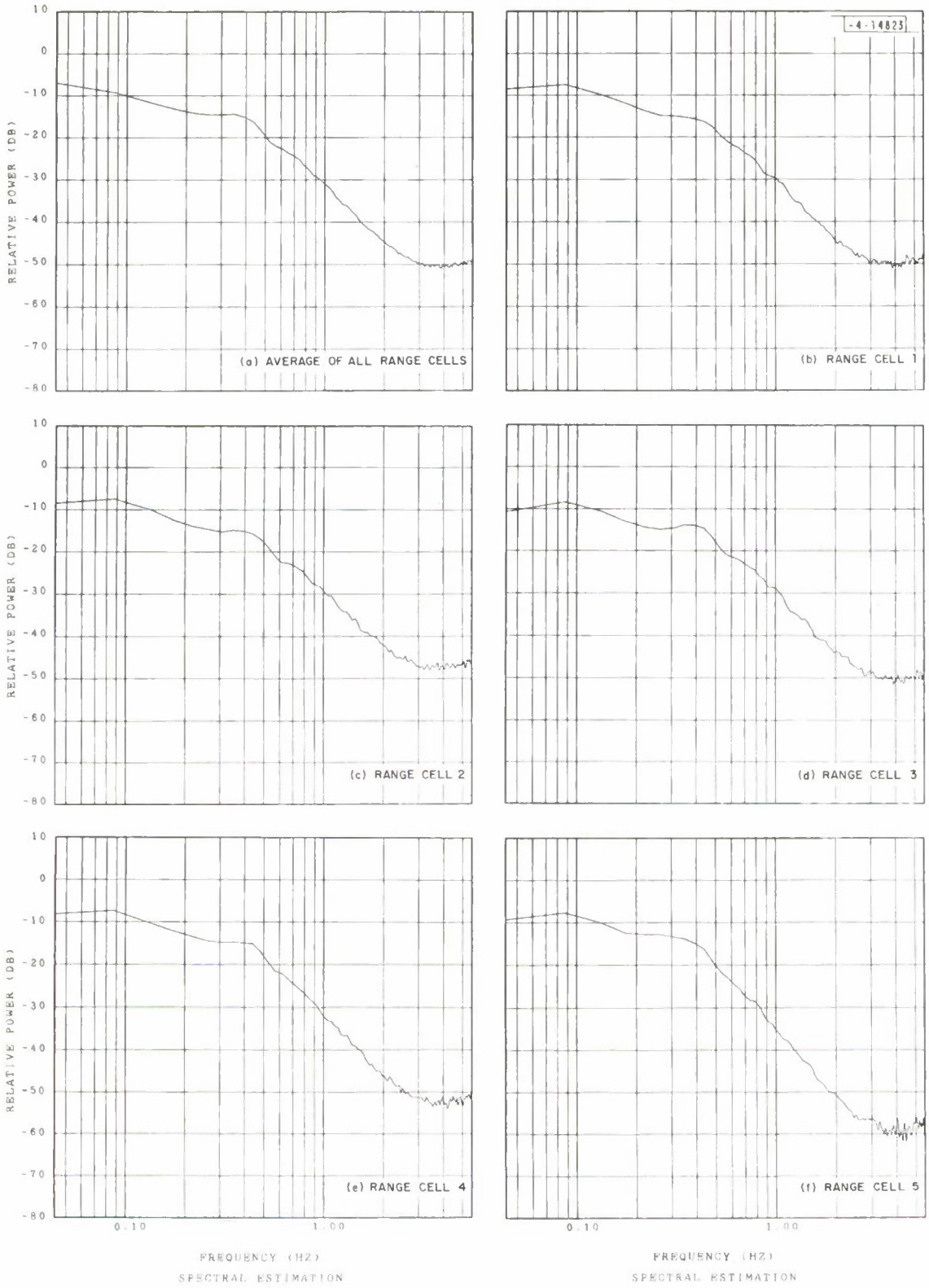

Fig. II-11. Clutter from area 1. DFT length = 256, resolution = 0.0659 Hz, sampling rate = 11.25 Hz. (a) DFTs averaged = 270; (b) through (f) DFTs averaged = 54.

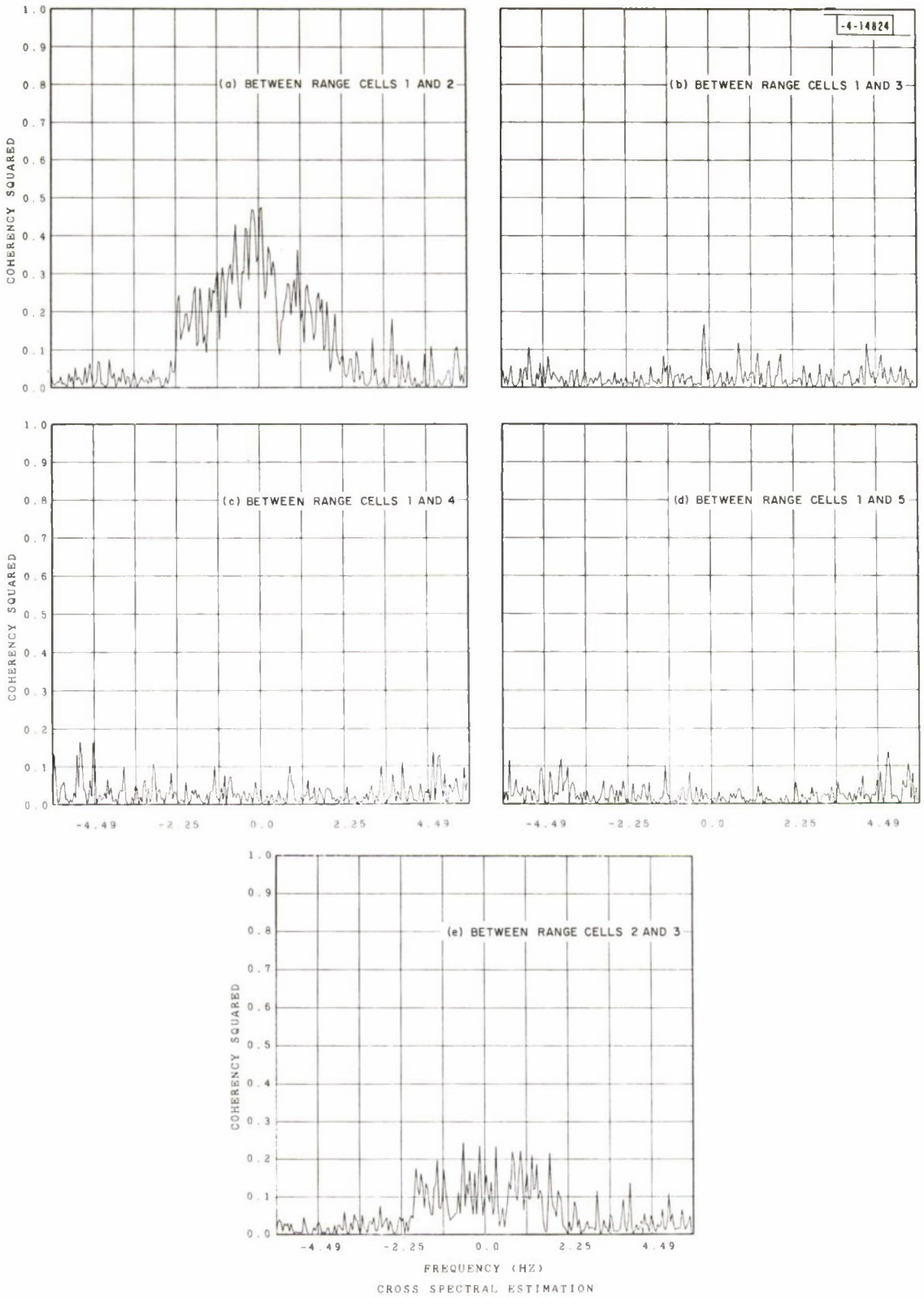

Fig. II-12(a-e). Clutter from area 1; correlation between range cells.

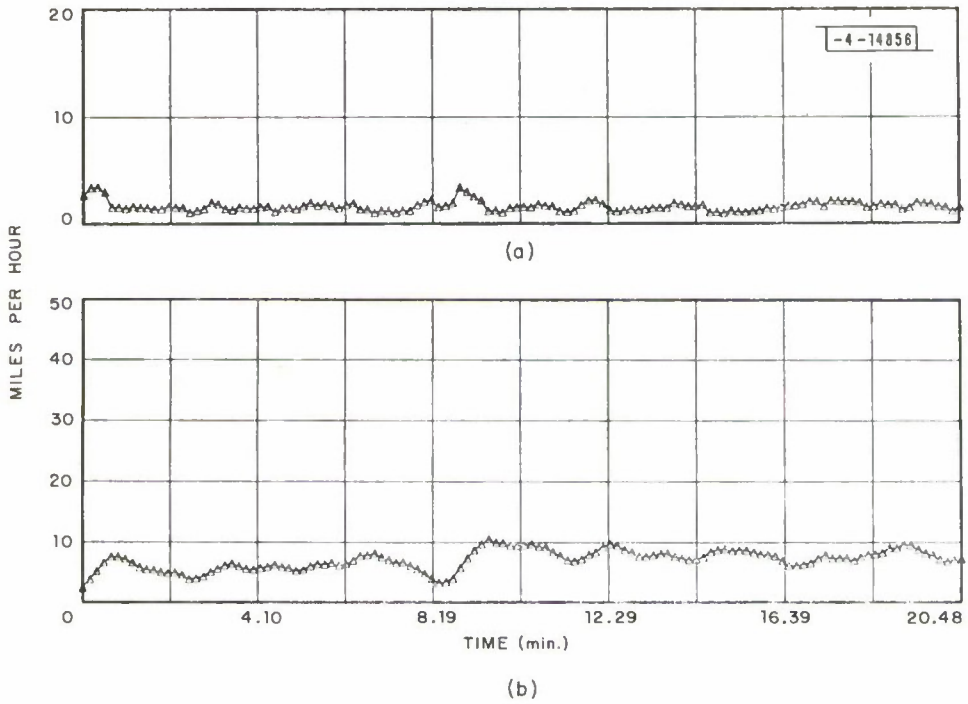

Fig. II-13. Clutter from area 1; wind speed at antenna tower. (a) Running standard deviation of wind; (b) running average of wind.

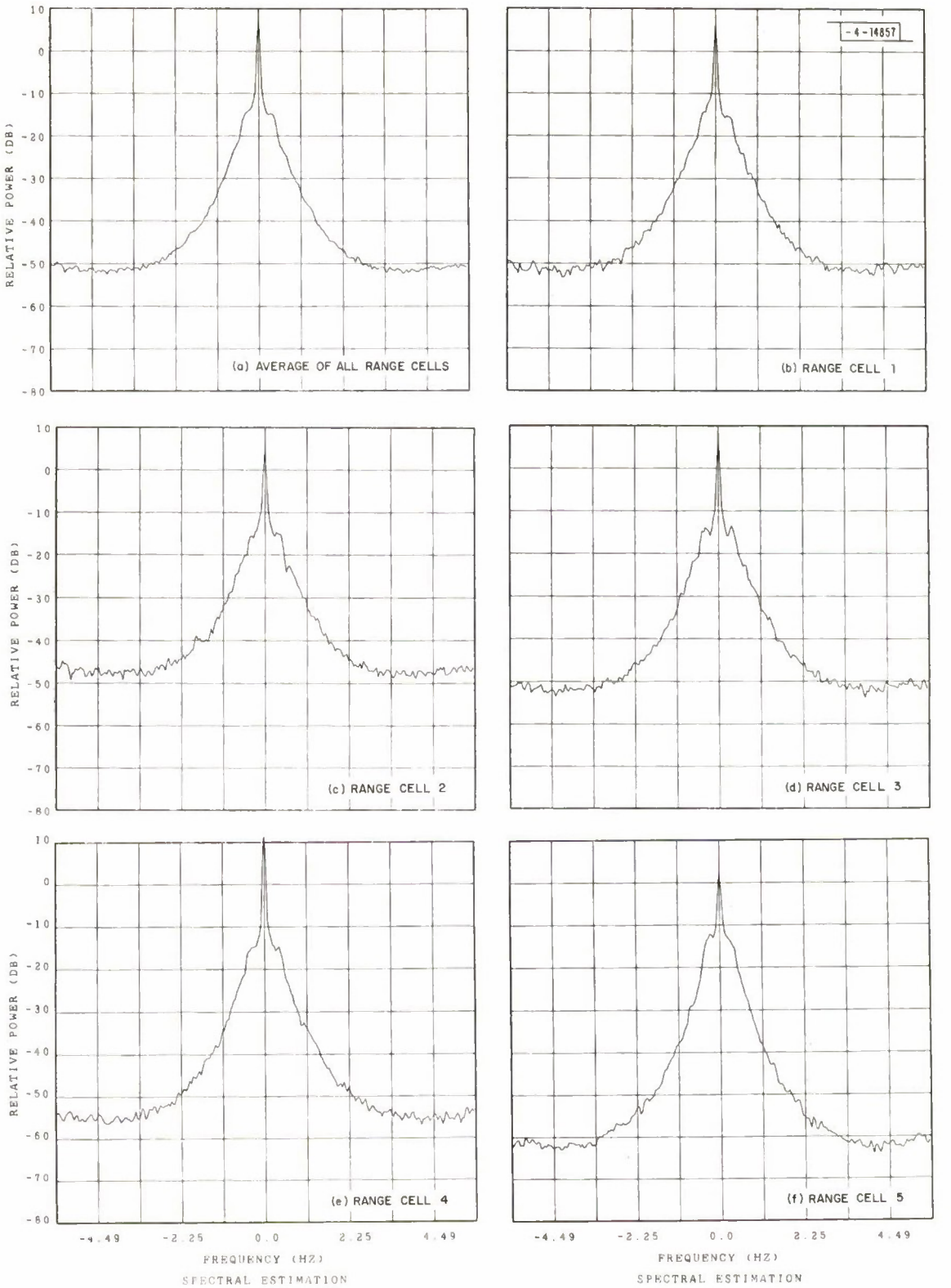

Fig. II-14. Clutter from area 1. DFT length = 256, resolution = 0.0659 Hz, sampling rate = 11.25 Hz. (a) DFTs averaged = 270; (b) through (f) DFTs averaged = 54.

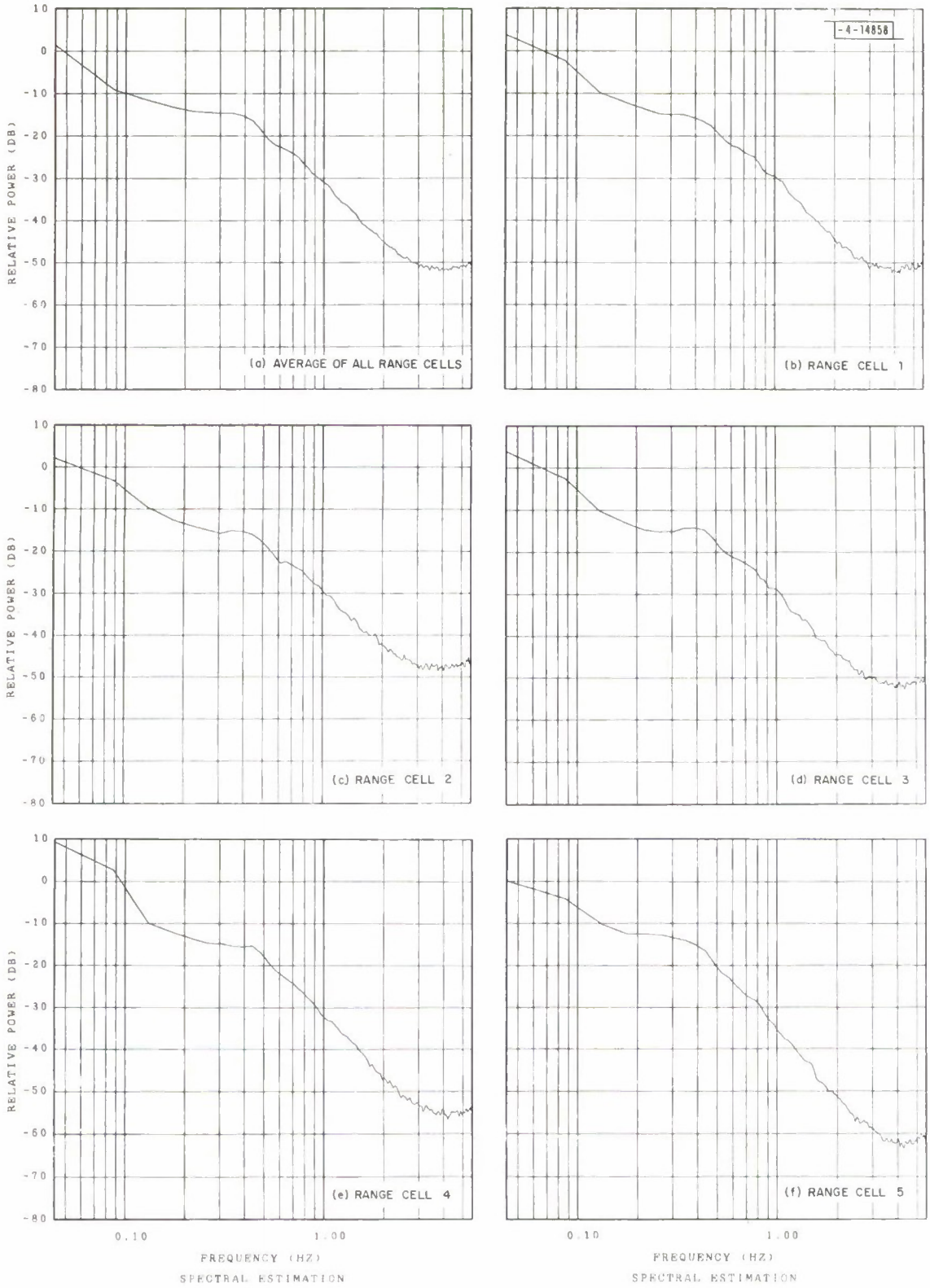

Fig. II-15. Clutter from area 1. DFT length = 256, resolution = 0.0659 Hz, sampling rate = 11.25 Hz. (a) DFTs averaged = 270; (b) through (f) DFTs averaged = 54.

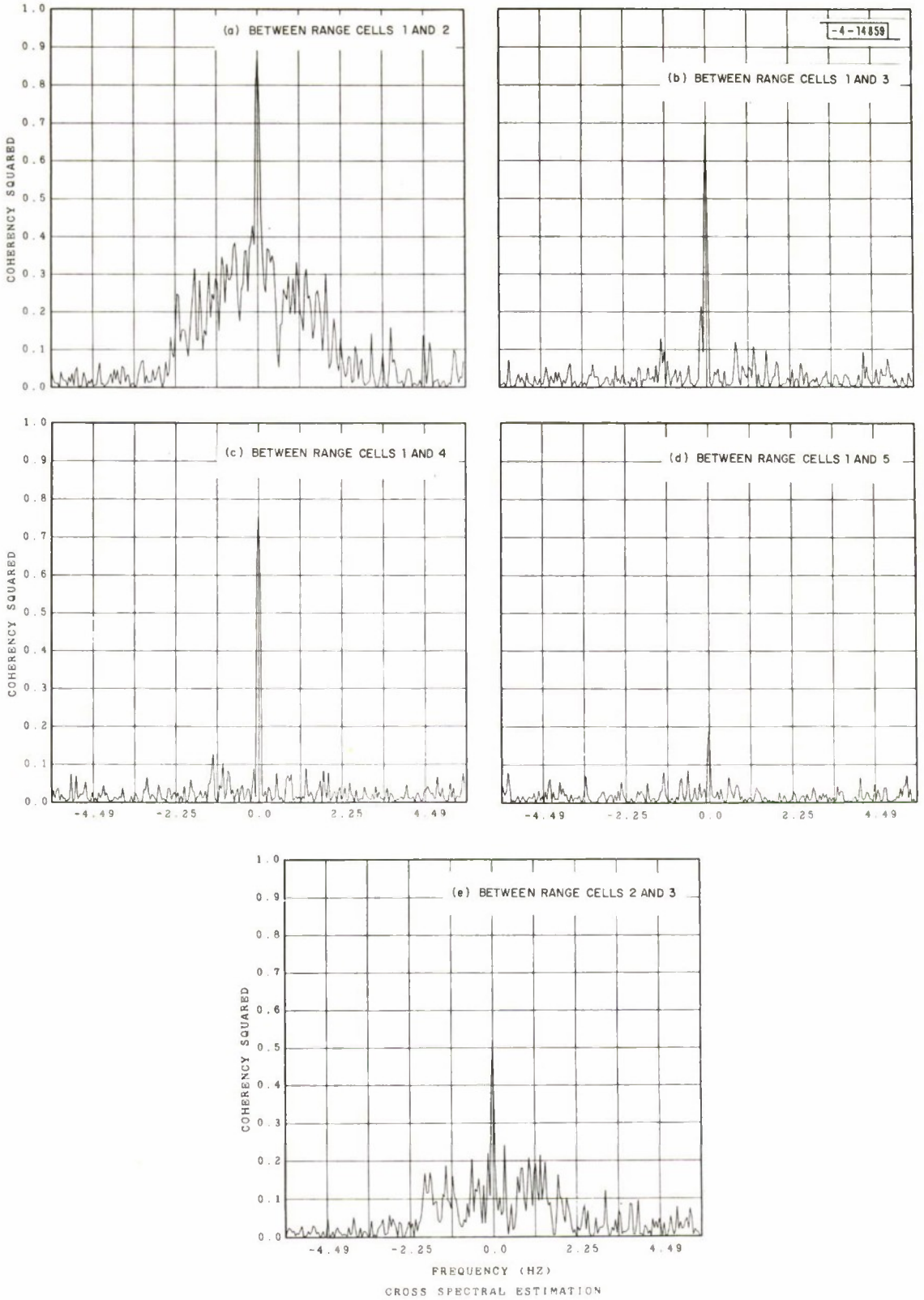

Fig. II-16(a-e). Clutter from area 1; correlation between range cells.

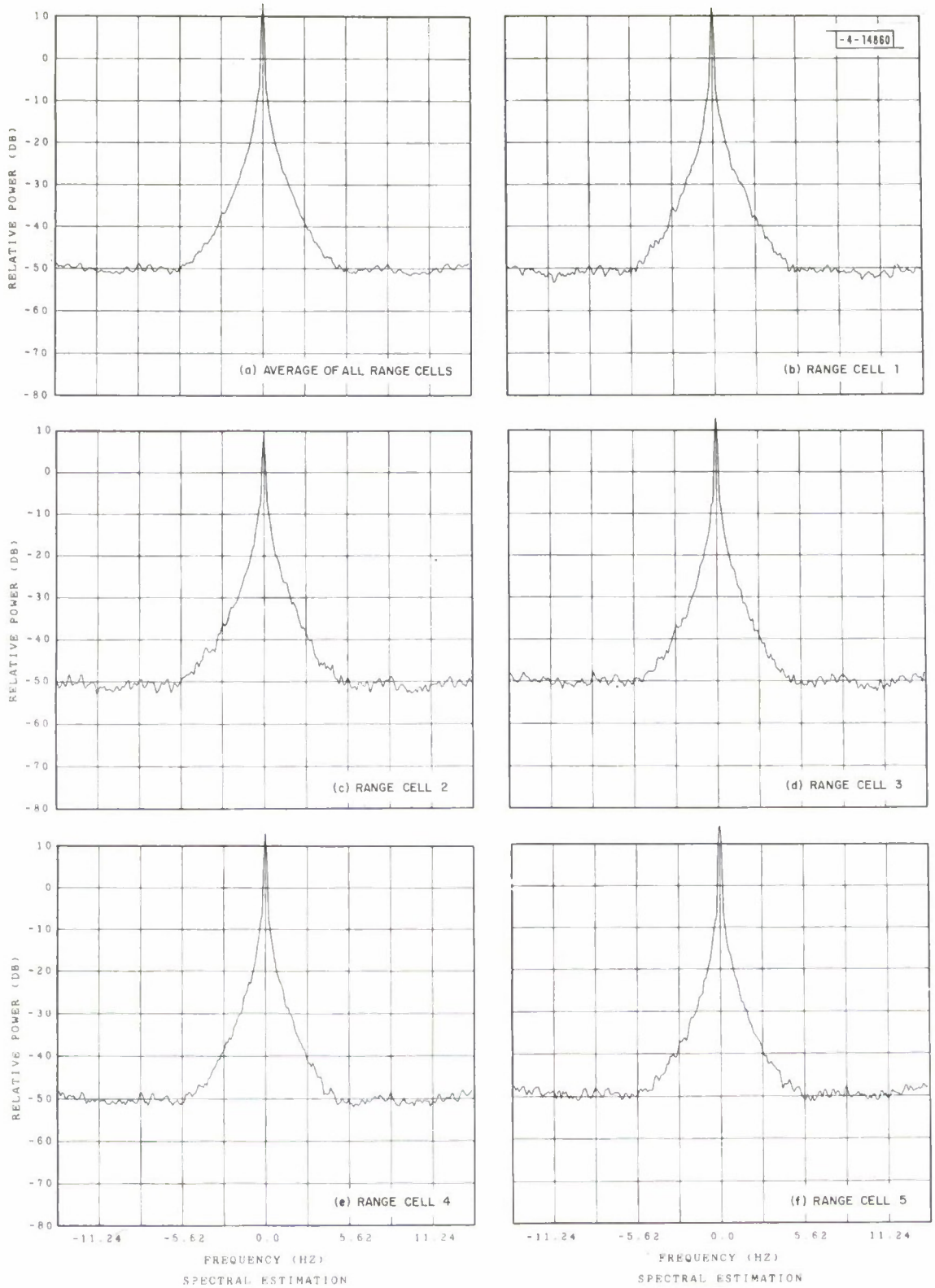

Fig. II-17. Clutter from area 2. DFT length = 256, resolution = 0.165 Hz, sampling rate = 28.12 Hz. (a) DFTs averaged = 270; (b) through (f) DFTs averaged = 54.

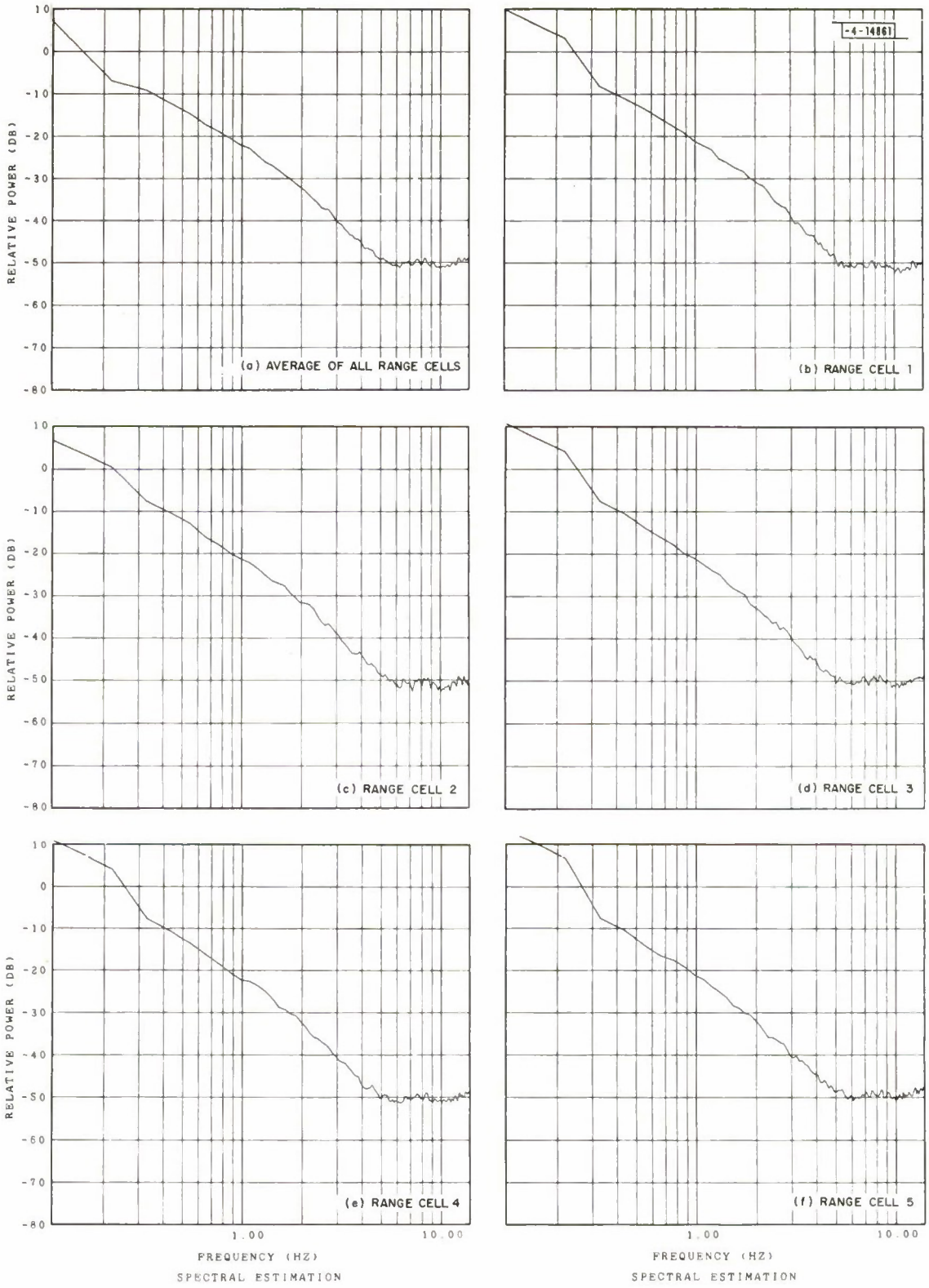

Fig. II-18. Clutter from area 2. DFT length = 256, resolution = 0.165 Hz, sampling rate = 28.12 Hz. (a) DFTs averaged = 270; (b) through (f) DFTs averaged = 54.

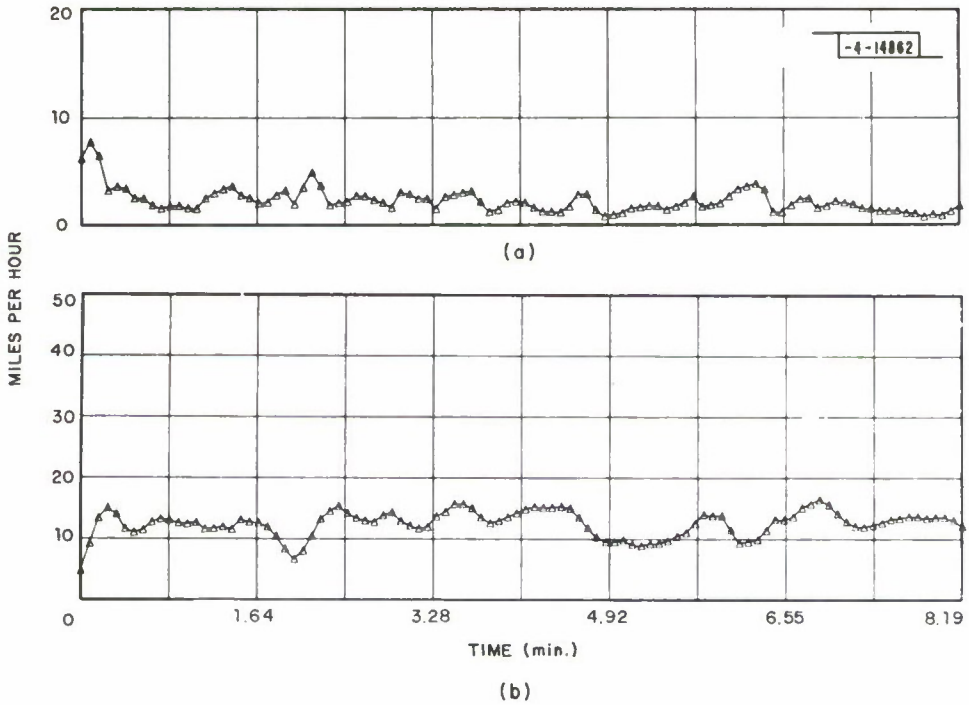

Fig. II-19. Clutter from area 2; wind speed at antenna tower. (a) Running standard deviation of wind; (b) running average of wind.

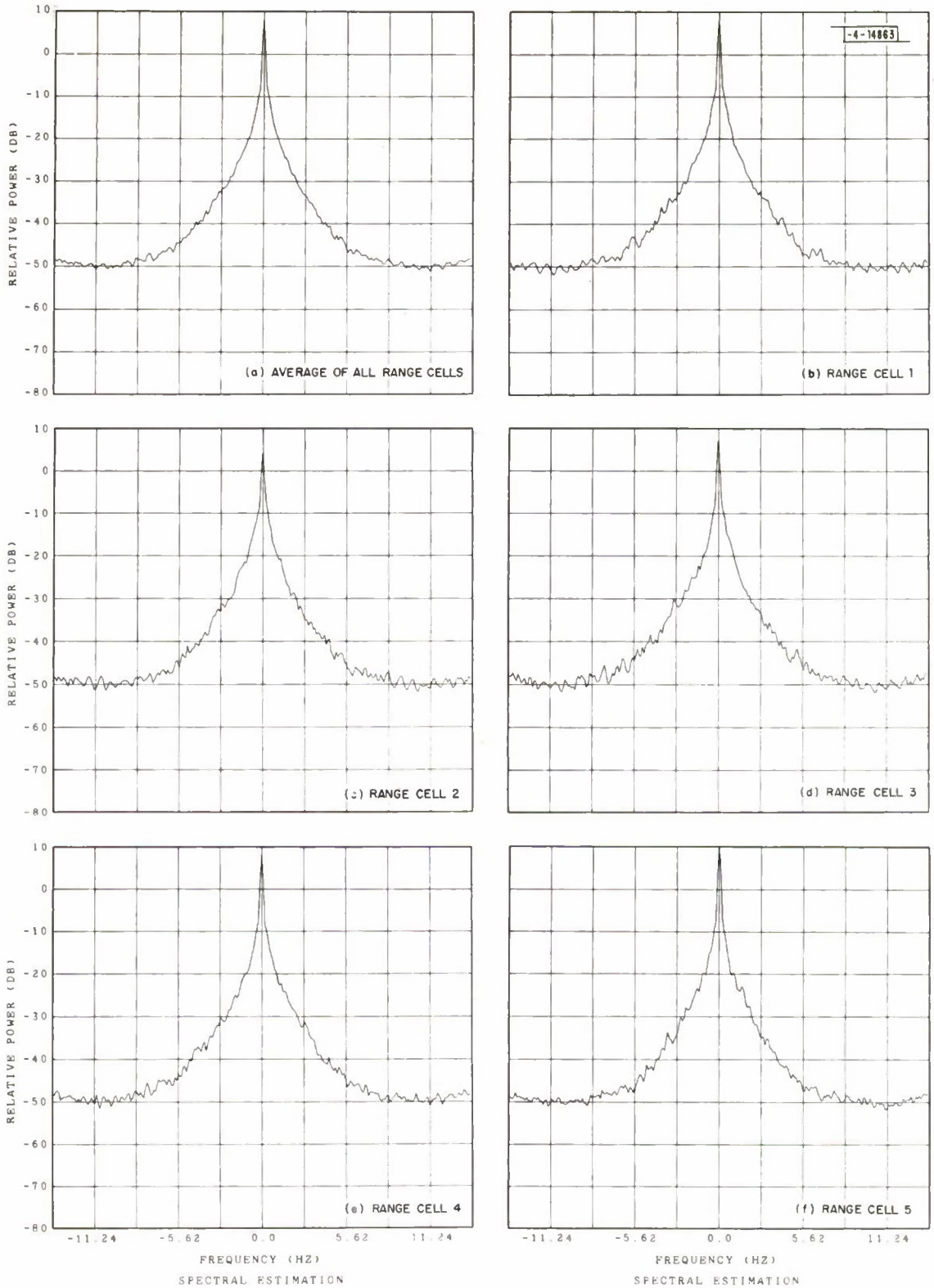

Fig. II-20. Clutter from area 2. DFT length = 256, resolution = 0.165 Hz, sampling rate = 28.12 Hz. (a) DFTs averaged = 265; (b) through (f) DFTs averaged = 53.

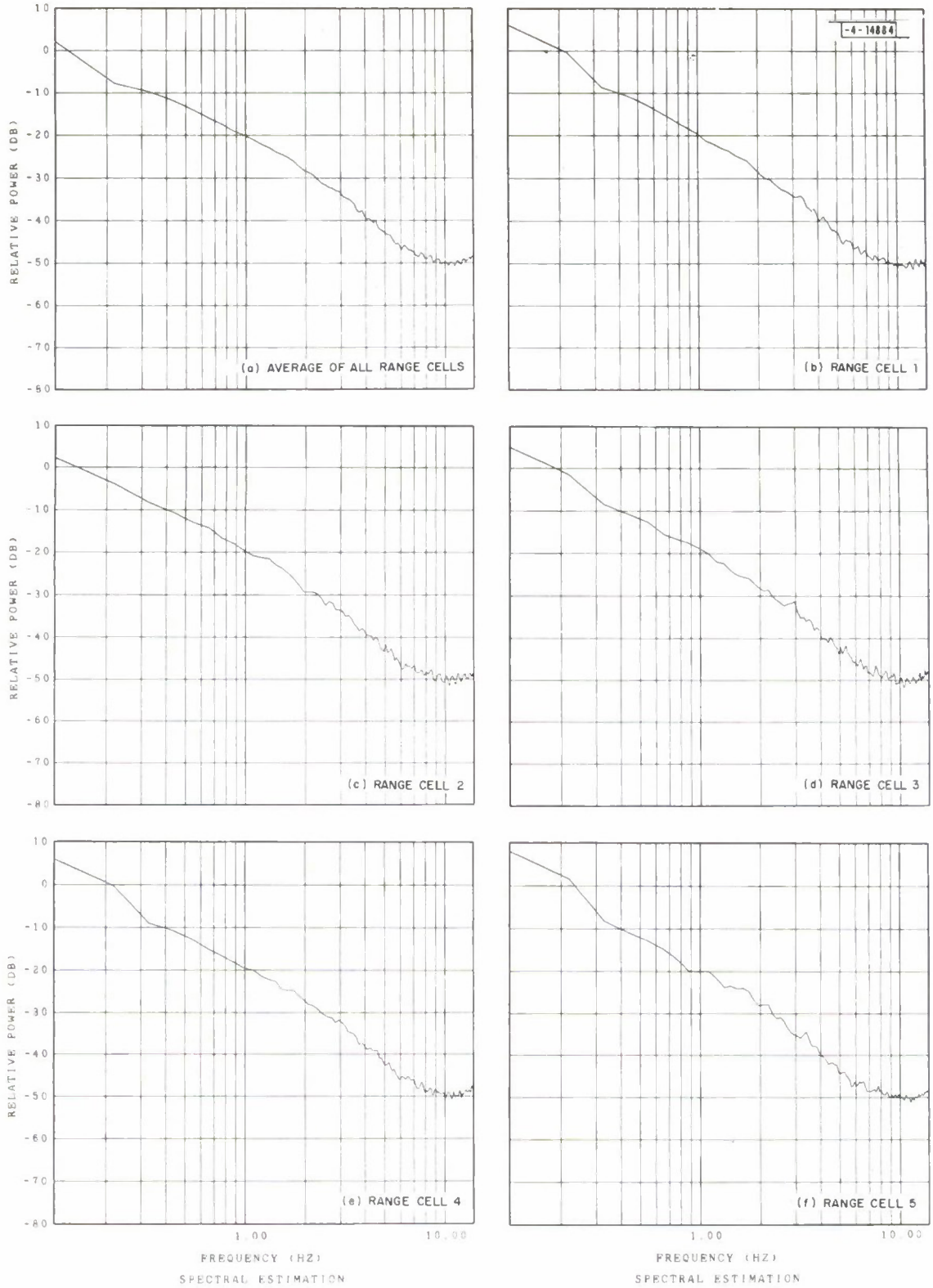

Fig. II-21. Clutter from area 2. DFT length = 256, resolution = 0.165 Hz, sampling rate = 28.12 Hz. (a) DFTs averaged = 265; (b) through (f) DFTs averaged = 53.

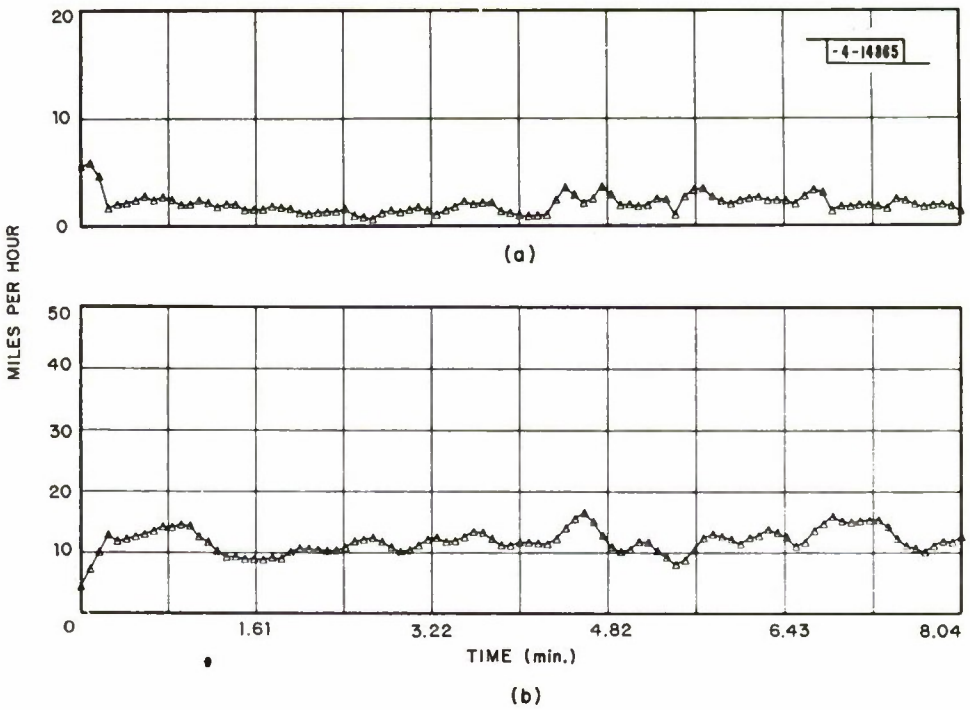

Fig. II-22. Clutter from area 2; wind speed at antenna tower. (a) Running standard deviation of wind; (b) running average of wind.

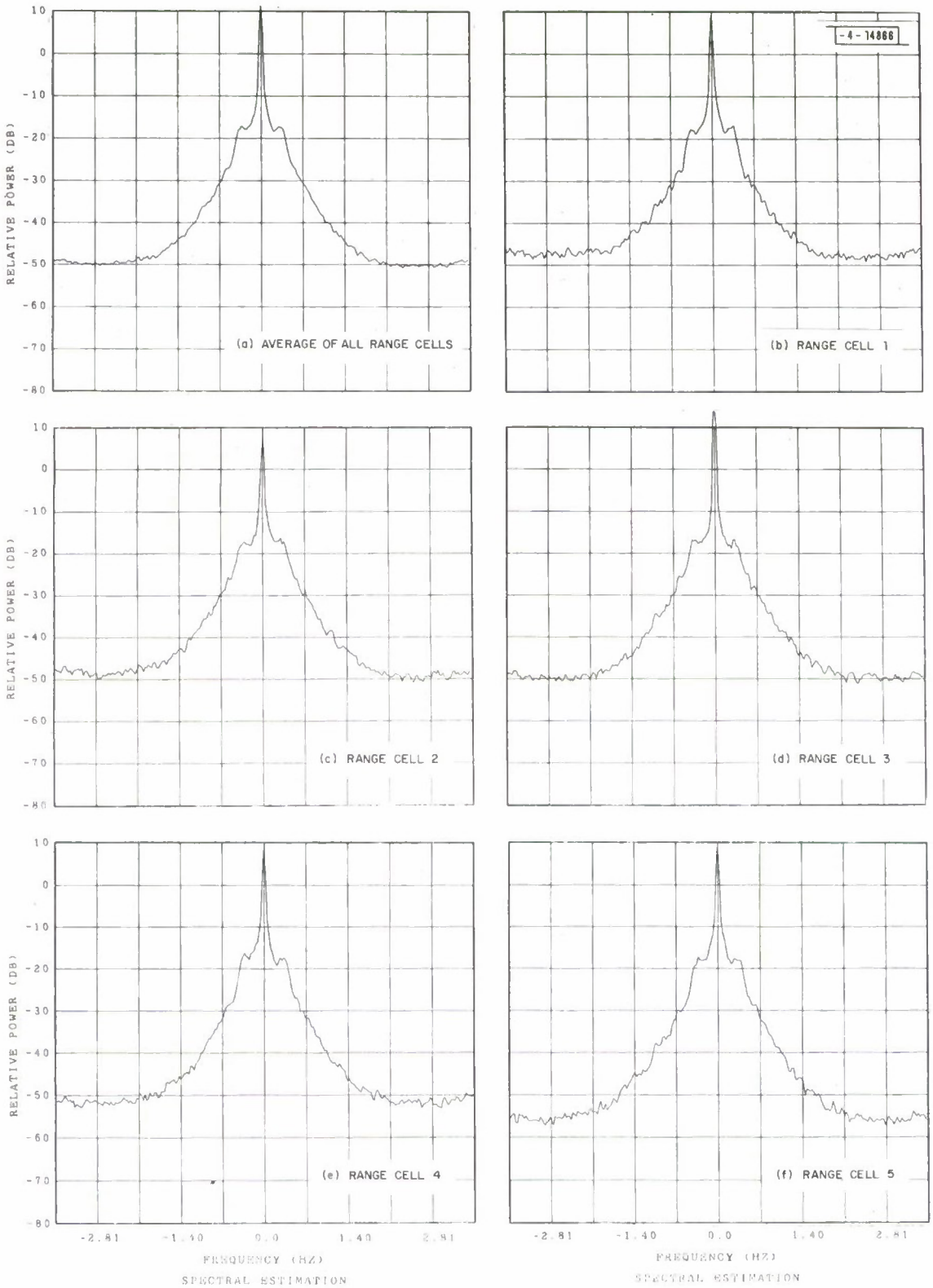

Fig. II-23. Clutter from area 3. DFT length = 256, resolution = 0.0412 Hz, sampling rate = 7.03 Hz. (a) DFTs averaged = 375; (b) through (f) DFTs averaged = 75.

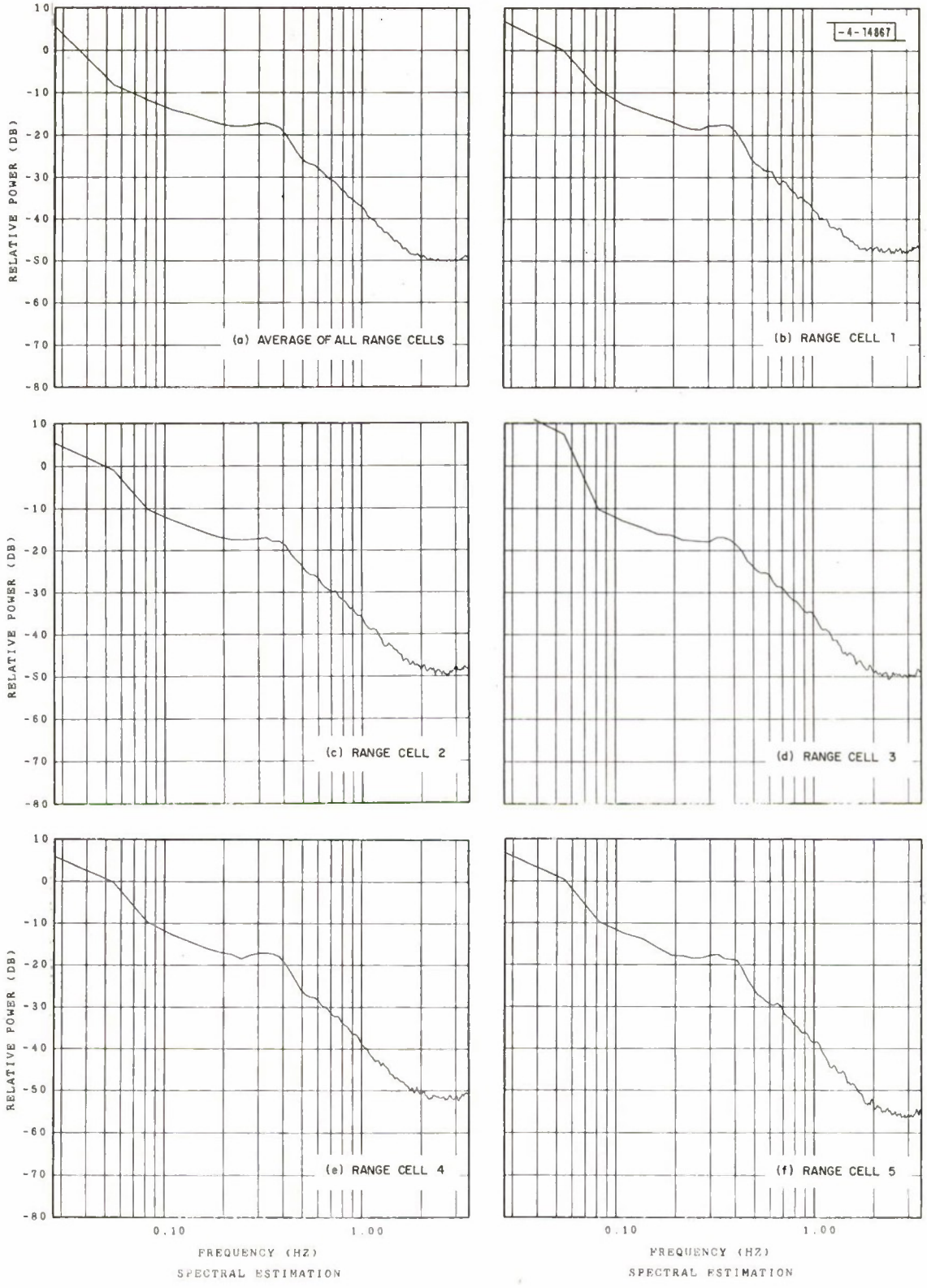

Fig. II-24. Clutter from area 3. DFT length = 256, resolution = 0.0412 Hz, sampling rate = 7.03 Hz. (a) DFTs averaged = 375; (b) through (f) DFTs averaged = 75.

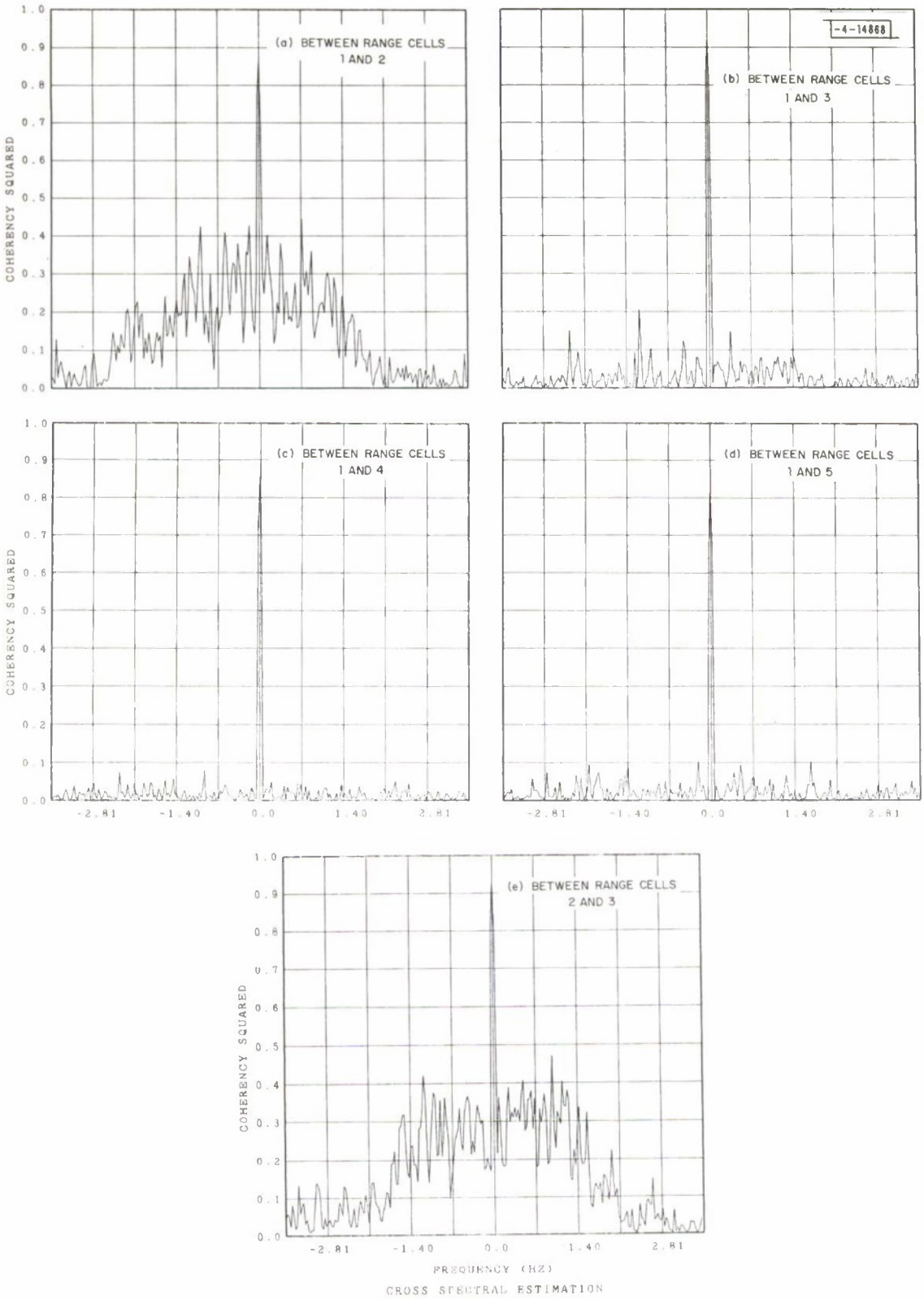

Fig. II-25(a-e). Clutter from area 3; correlation between range cells.

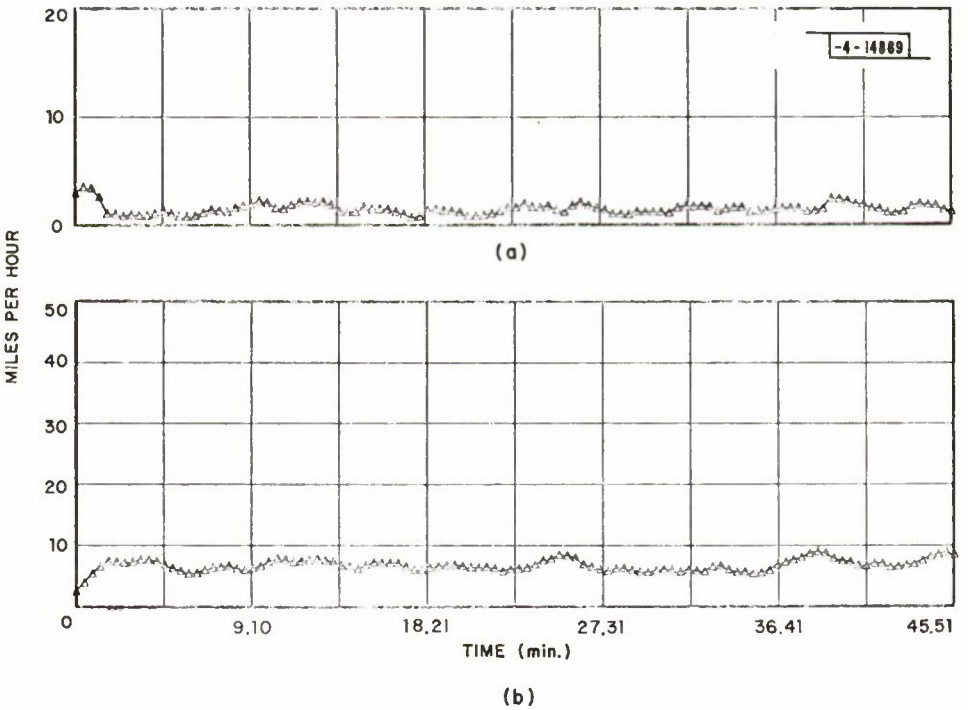

Fig. II-26. Clutter from area 3; wind speed at antenna tower. (a) Running standard deviation of wind; (b) running average of wind.

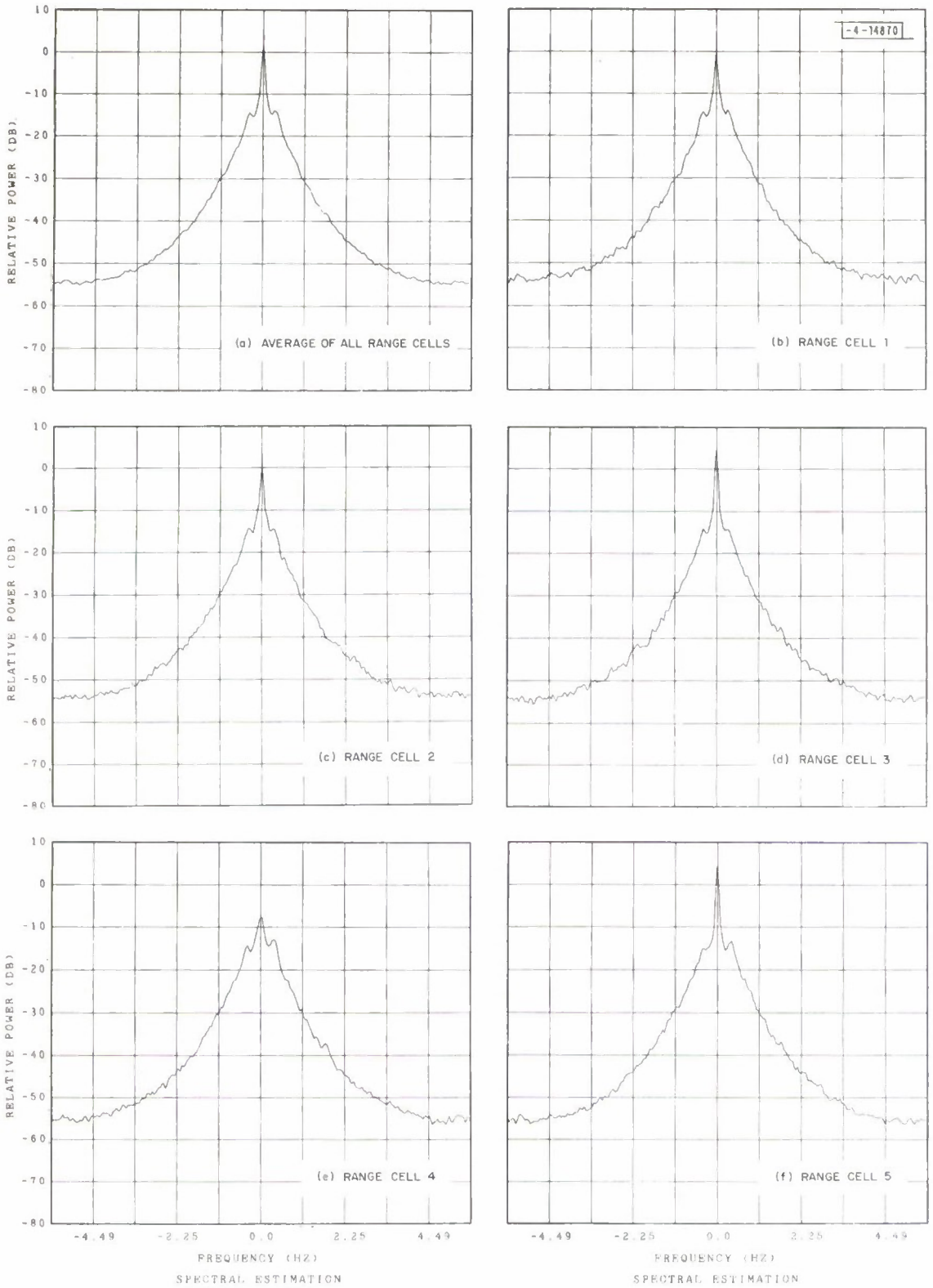

Fig. II-27. Clutter from area 3. DFT length = 256, resolution = 0.0659 Hz, sampling rate = 11.25 Hz. (a) DFTs averaged = 540; (b) through (f) DFTs averaged = 108.

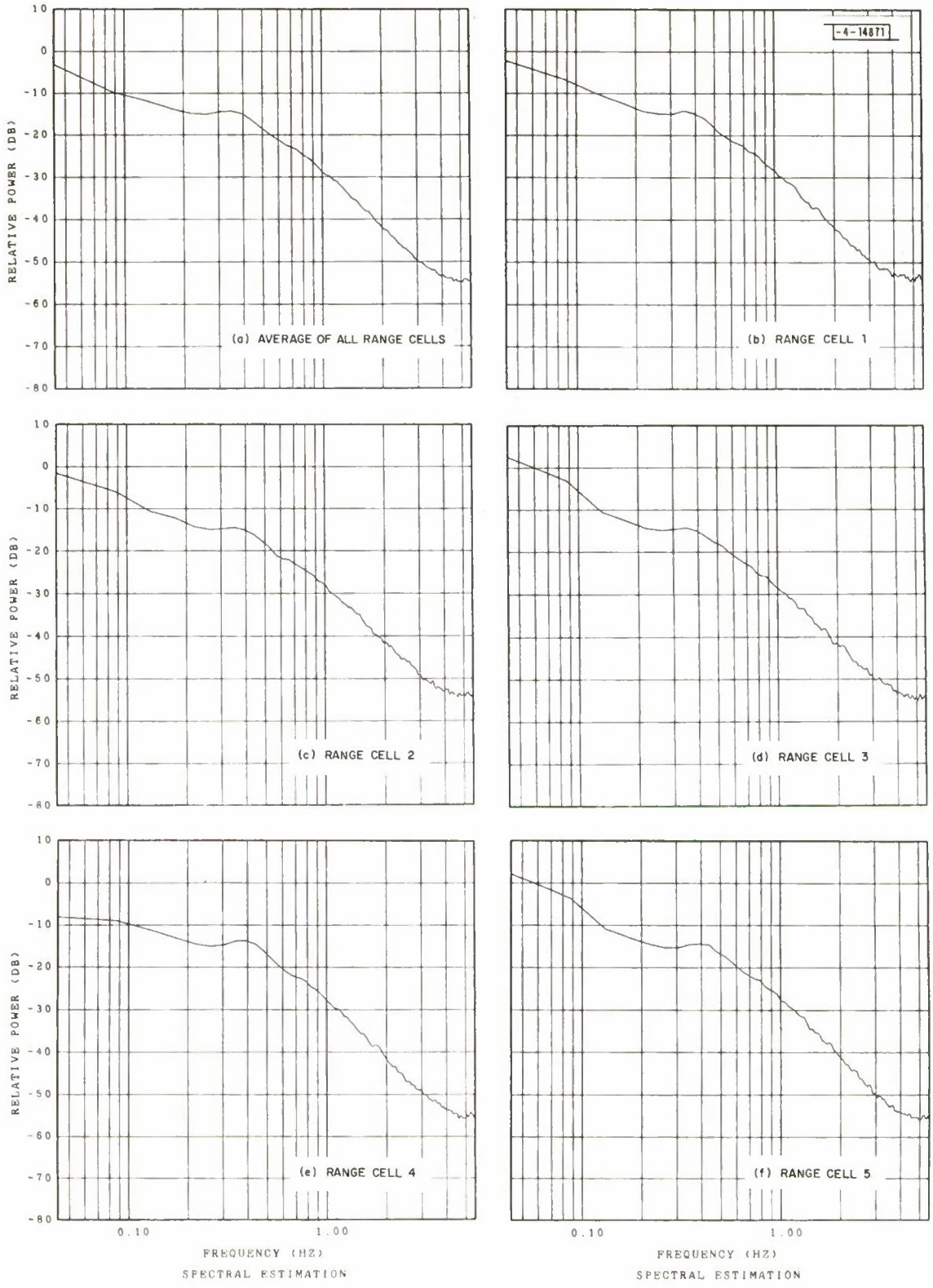

Fig. II-28. Clutter from area 3. DFT length = 256, resolution = 0.0659 Hz, sampling rate = 11.25 Hz. (a) DFTs averaged = 540; (b) through (f) DFTs averaged = 108.

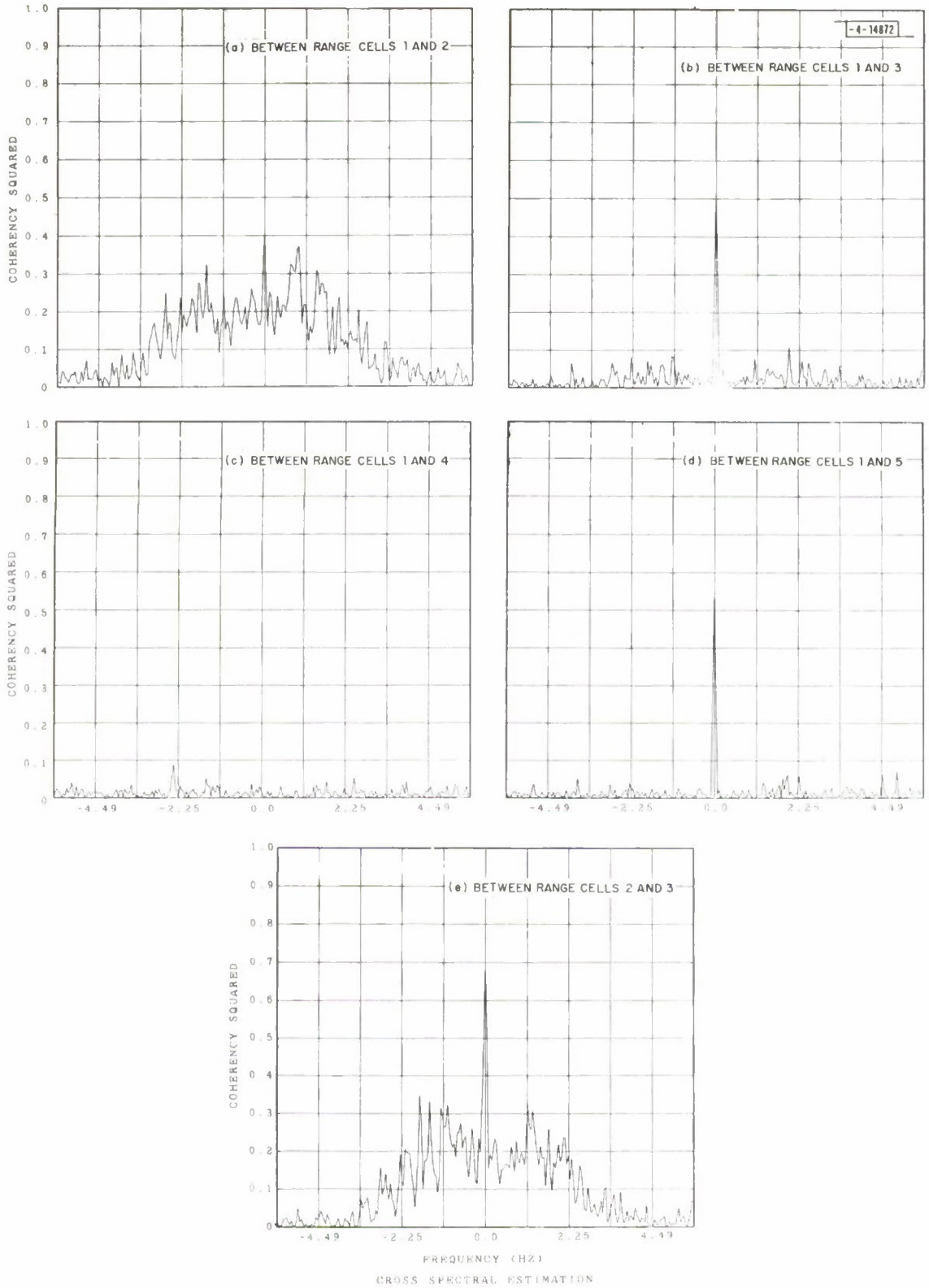

Fig. II-29(a-e). Clutter from area 3; correlation between range cells.

III. TARGET SPECTRUM FROM FOLIATED AREAS

R. D. Yates

A. Theory

In a forest, the incident electromagnetic energy is scattered from many points which are moving in a bound manner due to the wind turbulence. This produces an electromagnetic field across a range-azimuth cell which is both spatially and time varying. As a target travels through the range cell, this varying electromagnetic field modulates its return and produces an observed signal with a bandwidth greater than the bandwidth of the same target return in a clear region.

A detailed study of this problem is presented in Ref. 6. The purpose of this section is to recast the results in radar terminology and to summarize them. The forest model used is identical to that used to model the clutter returns as described in Sec. II-A.

A point target with a polarizability factor $\mathcal{P}$ is assumed to be traveling in a radial direction toward the radar with a constant velocity v. Although a general expression for the target spectrum is derived, it will be assumed that the random permittivity $\epsilon(\underline{r}, t)$ is statistically homogeneous and isotropic in all directions, and statistically stationary in time.

Let $X(t) = I(t) + jQ(t)$ represent the complex envelope of the range-gated video signal from a pulse-doppler radar such as the Long Range Demonstration Radar (LRDR). Assuming that the compressed pulse duration is greater than the time spreading due to multipath, the return from the point target may be expressed as

$$X(t) = G_r^{1/2} \cdot P_T^{1/2} \cdot P\left[\frac{2v}{c}(t - t_o)\right] \cdot a(t) \qquad \text{(III-1)}$$

in which

G_r = receiver gain

P_T = target received peak power

$P(t)$ = compressed pulse which defines the range cell with $\max |P(t)| = 1$

$a(t)$ = unit power modulation process due to target motion and varying field across range cell.

In general, the random process $a(t)$ will not be statistically stationary. However, if the random permittivity $\epsilon(\underline{r}, t)$ is statistically homogeneous and isotropic in $\underline{r}$ and statistically stationary in t, then as long as the target's velocity is constant, $a(t)$ will be a stationary random process. For a target traveling at a constant velocity v in a radial toward the radar, in a clear area, $a(t)$ is then equal to $\exp\{j[(4\pi/\lambda)vt + \Theta]\}$, where Θ is a random variable uniformly distributed between $-\pi$ and π radians.

The function $P[(2v/c)t]$ represents a time gating pulse, and corresponds to the complex envelope of the compressed transmitted signal. In the LRDR, since the time sidelobes of the compressed pulse are at least 30 dB below the main peak, $P(t)$ can be taken as the complex envelope of the signal that is fed to the mixers when the input signal is the basic pulse that defines a bit in the code.

It has been assumed that the time multipath spreading of the basic bit pulse is small. If this is not the case, then the duration of $X(t)$ will be greater than $P[(2v/c)t]$. However, for a homogeneous, isotropic forest, the energy spectral density of $X(t)$ will not be changed.

The targets' received peak power P_T can be expressed as

$$P_T = P_o \cdot G \cdot A \cdot \sigma_T \cdot F_T \tag{III-2}$$

in which

P_o = transmitted peak power

G = one-way antenna gain

A = antenna aperture = $G\lambda^2/4\pi$

σ_T = target cross section in square meters

F_T = two-way target propagation factor.

The antenna gain G has been defined in Sec. II-A, Eq. (II-5). As for the clutter case, $\sigma_T F_T$ cannot be factored; their product is given as

$$\sigma_T F_T = \frac{\left(\frac{h_a - h_f}{\lambda}\right)^4}{R^8} \cdot \frac{4\pi}{\epsilon_o^2(\eta^2 - 1)^2} \cdot |g(h_T)|^2 \cdot |\mathcal{P}|^2 \cdot (1 + P_{AC}) \tag{III-3}$$

in which

h_a = antenna height

h_f = forest height

λ = free-space wavelength

R = range to cell

ϵ_o = free-space permittivity

η = slab refractive index

$g(h)$ = ground lobing and attenuation factor

h_T = target height

P_{AC} = power in the random component of the target return due to multipath

$\mathcal{P}$ = targets' polarizability.

The function g(h) represents the effects of attenuation and ground lobing within the dielectric slab and is given by Eq. (II-9). Although it is not possible to factor the product $\sigma_T F_T$, Eq. (III-3) contains three propagation terms as given by Eq. (II-17).

The function a(t) in Eq. (III-1) represents the modulation due to the target's motion and varying field across the range cell, and has a power spectral density $S_a(f)$ as follows:

$$S_a(f) = \frac{\delta(f - f_d) + S_{AC}(f)}{1 + P_{AC}} \tag{III-4}$$

in which

f_d = doppler frequency = $2v/\lambda$

$\delta(f)$ = delta function

$S_{AC}(f)$ = multipath contribution spectrum

$$P_{AC} = \int_{-\infty}^{\infty} S_{AC}(f)\, df.$$

In Eq. (III-4), the spectrum of the direct path to the target is the impulse at the doppler frequency f_d, while the contribution due to the multipath is given by $S_{AC}(f)$. The spectrum $S_a(f)$ of the random process a(t) has been normalized to unit power.

The multipath component spectrum can be written as

$$S_{AC}(f) = \int_0^1 S_o(u)\, S_w\left(\frac{4\pi}{\lambda}\eta\sqrt{1-u}, f - \eta f_d u\right) du \tag{III-5}$$

in which

$$S_o(u) = \frac{(2\pi)^5}{\lambda^4 \epsilon_o^2 \alpha} \cdot \beta(\sqrt{1-u}) \cdot \varphi\left(\frac{4\pi}{\lambda}\eta\sqrt{1-u}\right) \tag{III-6}$$

where

$$\beta(x) = \frac{\pi}{4}(3 + 2x^2 + 3x^4) \tag{III-7}$$

and $\varphi(\underline{k})$ is the spatial spectrum of the random permittivity and is defined as

$$\varphi(\underline{k}) = \iiint C(\underline{r})\, e^{-j\underline{r}\cdot\underline{k}} d^3\underline{r}$$

$$= \varphi(|\underline{k}|) \text{ due to statistical homogeneity and isotropy} \tag{III-8}$$

where $C(\underline{r})$ is the correlation function of the random permittivity and is defined as

$$C(\underline{r}) = E\{\epsilon(\underline{R}, t)\, \epsilon^*(\underline{R} - \underline{r}, t)\}$$

$$= C(|\underline{r}|) \text{ due to statistical homogeneity and isotropy and temporal stationarity} \tag{III-9}$$

The function $S_w(k, f)$ in Eq. (III-5) represents the effects of the motion of the scatterers due to the velocity field $\underline{V}(\underline{r}, t)$, and can be expressed as

$$S_w(k, f) = \int q(k, \tau)\, e^{-j2\pi f\tau}\, d\tau \quad . \tag{III-10}$$

in which

$$q(k, \tau) = E\left(\exp\{jk\,[D(t) - D(t-\tau)]\}\right) \quad . \tag{III-11}$$

In Eq. (III-11), D(t) is a displacement random process and is not a function of position, since the forest has been taken to be statistically homogeneous and isotropic in all directions. The correlation function $m(\tau)$ defined by Eq. (II-28) is seen to be equal to $q\,[(4\pi/\lambda), \tau]$. Hence, the unit power clutter spectrum is then equal to $S_w\,[(4\pi/\lambda), f]$.

The first simplification of Eq. (III-5) is when the scatterers are not in motion, so that $S_w(k, f) = \delta(f)$. Hence, the power spectral density $S_{AC}(f)$ given by Eq. (III-5) reduces to

$$S_{AC}(f) = \frac{S_o\left(\frac{f}{\eta f_d}\right)}{\eta f_d} \qquad \text{for } 0 \leqslant f \leqslant \eta f_d$$

$$= 0 \text{ elsewhere} \quad . \tag{III-12}$$

Thus, the power spectral density of the random process a(t) can be written as

$$S_a(f) = \frac{1}{1 + P_{AC}} \left[\delta(f - f_d) + \frac{(2\pi)^5}{\lambda^4 \cdot \epsilon_o^2 \alpha} \cdot \beta\left(\sqrt{1 - \frac{f}{\eta f_d}}\right) \cdot \varphi\left(\frac{4\pi}{\lambda} \eta \sqrt{1 - \frac{f}{\eta f_d}}\right)\right]$$

$$\text{for } 0 \leqslant f \leqslant \eta f_d \tag{III-13}$$

in which $\beta(x)$ and $\varphi(k)$ are defined by Eqs. (III-7) and (III-8), respectively.

It is seen that the target spectrum contains no frequencies above the doppler frequency f_d, because the target is traveling in a radial direction toward the radar. The power P_{AC} due to the multipath is inversely proportional to α, the attenuation factor within the forest. Hence, for a forest with thick underbrush, one would expect the impulse component in Eq. (III-13) to dominate. For a telephone-type forest with very little underbrush, the random component $S_{AC}(f)$ would be the dominant term.

Since the observed signal X(t) given by Eq. (III-1) is a time-gated version of the process a(t), we must consider the energy spectral density of X(t) defined as follows:

$$E_x(f) = E\left\{\left|\int X(t)\, e^{-j2\pi ft}\, dt\right|^2\right\} \tag{III-14}$$

$$= b \cdot \int S_a(\nu) |F(f - \nu)|^2 \, d\nu \tag{III-15}$$

where b is a constant, and F(f) is the Fourier transform of the gating pulse used. Hence, the resolution of the random component $S_{AC}(f)$ of a(t) will depend on the ratio of the bandwidth of $S_{AC}(f)$ to the bandwidth of $|F(f)|^2$. If this ratio is large, then $E_x(f)$ can be approximated as follows:

$$E_x(f) = b' \left[W(f - f_d) + S_{AC}(f)\right] \tag{III-16}$$

in which b' is a constant, and W(f) is a unit area window function defined as

$$W(f) = \frac{|F(f)|^2}{\int |F(f)|^2 \, df} \quad . \tag{III-17}$$

The other simplification of Eq. (III-5) results when the target velocity is assumed to be zero and wind turbulence is present. Hence,

$$S_{AC}(f) = \int_o^1 S_o(u)\, S_w\left(\frac{4\pi}{\lambda} \eta \sqrt{1 - u}, f\right) du \quad . \tag{III-18}$$

The normalized clutter power spectral density is given as $S_w\,[(4\pi/\lambda), f]$. Assume that the phase modulation index $\mu = 4\pi\sigma/\lambda$, given by Eq. (II-20), is less than 1. Then, Eq. (III-4) can be expressed as

$$S_a(f) = (1 + P_{AC})^{-1} \cdot \left\{\left[1 + P_{AC}\left(1 - \overline{\mu^2}\right)\right] \delta(f) + P_{AC} \cdot \overline{\mu^2} S_d(f)\right\} \tag{III-19}$$

in which $\delta(f)$ is the delta function, $S_d(f)$ is the normalized displacement process defined by Eq. (II-40), and $\overline{\mu^2}$ is a mean square phase modulation index defined as follows:

$$\overline{\mu^2} = \left(\frac{4\pi\sigma\eta}{\lambda}\right)^2 \cdot \frac{\int_0^1 uS_o(1-u)\,du}{\int_0^1 S_o(u)\,du} \quad . \tag{III-20}$$

The function $S_o(u)$ is given by Eq. (III-6), and P_{AC} [the power in the AC component of a(t)] is given as

$$P_{AC} = \int_0^1 S_o(u)\,du \quad . \tag{III-21}$$

It follows from Eq. (III-20) that $\overline{\mu^2} \leqslant \mu^2$, where μ is the phase modulation associated with the clutter spectrum. Since the non-impulse part of Eq. (III-19) is due mainly to forward scattering, one would expect that the DC-to-AC power ratio in $S_a(f)$ would be greater than that of the clutter spectrum.

B. Experiments

In this section, several experiments are described which were performed to verify the theoretical results given in Sec. A above.

1. Transponder Returns

A coherent transponder described in Sec. III-F-1 in Vol. 1 was used as a point target. Its antenna is horizontally polarized and essentially omnidirectional. The received signal is amplified, delayed by 20 μsec, and frequency shifted by $(256 \times 555.6 \times 10^{-6})^{-1} = 7.03$ Hz. The reason for the frequency shift is to ensure that the target return does not overlap the clutter return in frequency. Amplification of the signal was necessary in order to ensure that the target spectrum be well above the receiver noise. The transponder was pulled at a constant velocity at a fixed height above the nominally flat ground within foliated areas.

a. Transponder Closed-Loop Stability

In order to determine the spectral purity of the transponder, a closed-loop stability test was performed. The low level coded gated RF from the LRDR was fed directly to the transponder via a circulator. The amplified, time, and frequency-shifted signals were then fed to the LRDR receiver input. Adequate attenuation was used to ensure that the transponder and LRDR receiver were operating linearly. Using the measurement mode of the LRDR, the compressed, range-gated, low-pass-filtered, quadrature video components were recorded on digital magnetic tape using the TAPWRITE system described in Sec. III-F-3 in Vol. 1.

An estimate of the power spectral density of the transponder signal is given in Fig. III-1. The main line is at +7.03 Hz while its image at −7.03 Hz is 28 dB below it. This image is due to phase and amplitude errors in the quadrature channels. The other lines, which are at least 38 dB below the main line, appear to be due to the transponder's nonideal digital frequency shifter. A closed-loop-stability test of the entire radar, as reported in Sec. II-D in Vol. 1, shows that there are no spurious signals present. These extra lines presented no major problems in the experiments to be discussed.

b. Spectrum Broadening Due to Multipath

In order to verify the nature of the power spectral density [as given by Eq. (III-13)] for the return from a point target in a foliated area, the transponder was used as the target.

The area chosen was several kilometers from the radar and consisted of trees with an average height of 40 feet with light foliage. The transponder traveled a distance of 90 feet in which a 50-foot range cell was centered. Eleven round trips were made so that some averaging of the data was possible.

The time data per pass were examined to isolate the section which contained the major return. A time-weighted FFT was performed on the data and successive FFTs were added incoherently to provide smoothing. If the number of points per FFT is denoted as $N = 2^n$, then the number of FFTs per pass was 1024/N.

The estimated spectrum for an inbound pass is shown in Figs. III-2, -3, and -4 for FFT lengths of 64, 256, and 1024, respectively. The corresponding spectrum for an outbound pass is shown in Figs. III-5, -6, and -7. It appears that Figs. III-3 and -6 show the best tradeoff between resolution and smoothing and, on examining them, it is seen that the inbound and outbound spectra are mirror images of each other about the offset frequency of 7.03 Hz. The predicted asymmetry about the offset doppler frequency of 8.21 Hz for the inbound pass and 5.85 Hz for the outbound pass is also present. Since the target doppler is 1.18 Hz and the 3-dB bandwidth about 1.4 Hz, the Q of the spectrum is then 0.85. Although this appears to be smaller than expected, it does correlate with the fact that the detection of a single man in the same range cell was very difficult. It appears that the multipath was severe enough to cause considerable broadening of the target spectrum.

In all these Figures, the component about zero frequency is the spectrum of the clutter from the range cell 20 μsec further out. The component about −7 Hz is due to the sideband unbalance of the system. The wind in the area of the range cell was minimal so that spectral broadening due to the motion of the scatterers can be neglected.

c. Spectrum Broadening Due to Wind

In order to determine the effect of the motion of the scattering centers on the spectra presented in Sec. b above, the transponder was placed in the center of the range cell and the resulting radar return was recorded. The theoretically predicted spectrum is given by Eq. (III-19).

The estimated spectrum is given in Fig. III-8, while the running mean and standard deviation of the wind velocity during the data recording time are given in Fig. III-9(a-b). Wind velocity was measured by an anemometer at the top of the antenna tower, and gives a relative measure of the wind conditions at the range cell since it was several kilometers away.

It is seen that the spectral broadening about the transponder offset frequency of 7.03 Hz occurs about 25 dB below the main line. Except for the clutter spectrum about zero frequency, the other lines present are due to the transponders digital frequency shifter as discussed in Sec. a above.

Based on the above results, it is seen that the effect of the wind on the spectra presented in Sec. b can be ignored. However, for high wind velocities, this may not be the case since the DC-to-AC power ratio of the spectrum given in Fig. III-8 would be greatly reduced.

2. Spectrum of Man in Woods

A man is an extended target vertically, so that some form of averaging of the field will occur. If the field statistics do not change significantly over the target's height, the spectrum of a man should be similar to that of a point target such as a transponder.

One man walked at a constant velocity in a radial direction with respect to the radar. The area consisted of trees with light underbrush. Several passes were made through the range cell to ensure smoothing of the spectral estimates. The range cell was several kilometers from the radar and in a different location from the transponder test area.

The spectral estimates with a frequency resolution of 0.659, 0.11, and 0.0549 Hz are given in Figs. III-10, -11, and -12 for an inbound pass, and in Figs. III-13, -14, and -15 for an outbound pass. It is clear that a frequency resolution of 0.659 Hz is not adequate in order to estimate the target spectrum. However, this case is presented here for comparison since the bandwidth of the coherent filters in the LRDR signal-processing scheme is 0.659 Hz. It appears that the best estimates are given by Figs. III-12 and -15.

On examining Fig. III-12 for the inbound pass, the definite asymmetry about the target doppler of 4.3 Hz is present. The 3-, 6-, and 10-dB bandwidth measures are 0.42, 0.93, and 1.46 Hz, respectively. Hence, the corresponding Qs, defined as the ratio of the doppler to bandwidth, are 10, 4.6, and 3, respectively. Since the bandwidth is proportional to the target's velocity, the Q is independent of target velocity.

The outbound spectrum is not a mirror image of the inbound spectrum as predicted by the theory and the transponder experiments. Due to the limited time allowed for science experiments, this problem was not investigated further. It could be attributed to poor velocity control of the target, and an incorrect centering of the range cell and data window.

3. Recommendations for Further Work

An extensive study of the spectrum of a target in a clear region was presented in Ref. 5. In addition, the spectrum of a man in foliage from one range cell was presented and it showed the asymmetry about the doppler frequency. The R^{-8} dependence of the received target power on range from foliated areas, as given by Eq. (II-3), was also verified. The refractive index η and attenuation α for several types of foliage were also estimated.

In this report, the transponder returns appear to have a spectrum with the correct properties as predicted by Eq. (II-13).

An extensive experimental program should be carried out to check the validity of the expressions for the target spectrum as presented in Sec. III-A. Different types of foliage should be studied to determine how they affect the target spectrum. Assuming that, over the observation time, the target's velocity is constant, it should be possible to characterize the foliage by a Q which can then be used in the design of the target filter bank.

Since the target return consists of a specular plus a random component, experiments should be designed to measure the ratio of the specular to random power. If the specular power is dominant, then the receiver should coherently integrate over the time-on-target. However, if the random component is dominant, then the receiver should coherently integrate over its coherence time and incoherently integrate over the time-on-target. This assumes that the target's velocity is constant over the time-on-target. Variations of target velocity will spread the appropriate spectrum further, and require wider bandwidth filters.

In order to predict receiver performance, the statistics of the target return must be known. If there is a great deal of multipath present, one might speculate that the random component of the target return is a Gaussian process. Experiments should be designed to estimate the statistics of the target return for various types of foliage.

Finally, more experiments are needed to determine the behavior of the received target power as a function of the type of foliage.

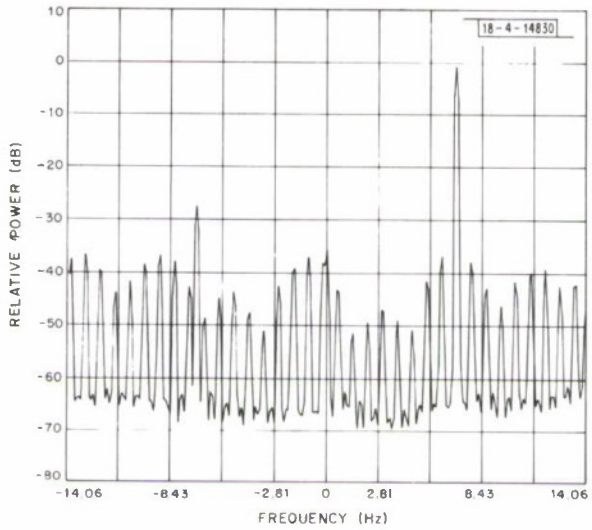

Fig. III-1. Transponder's closed-loop-stability spectrum. DFT length = 256, sampling rate = 28.12 Hz, resolution = 0.165 Hz, DFTs averaged = 54.

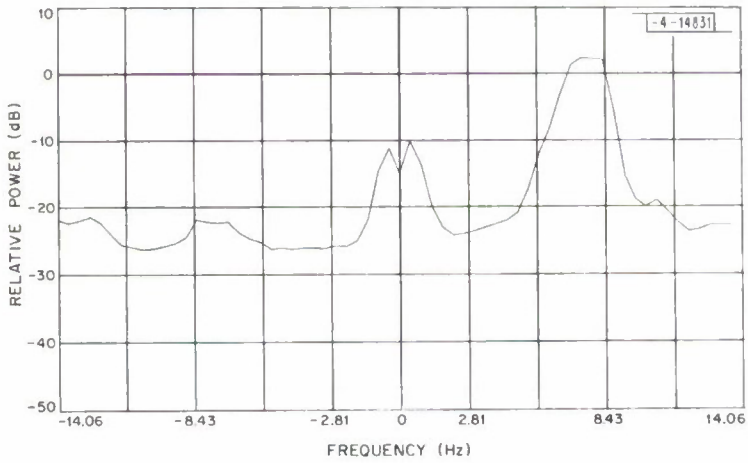

Fig. III-2. Spectrum of transponder in woods inbound. DFT length = 64, sampling rate = 28.12 Hz, resolution = 0.659 Hz, DFTs averaged = 176, target passes = 11, target velocity = 1.35 ft/sec.

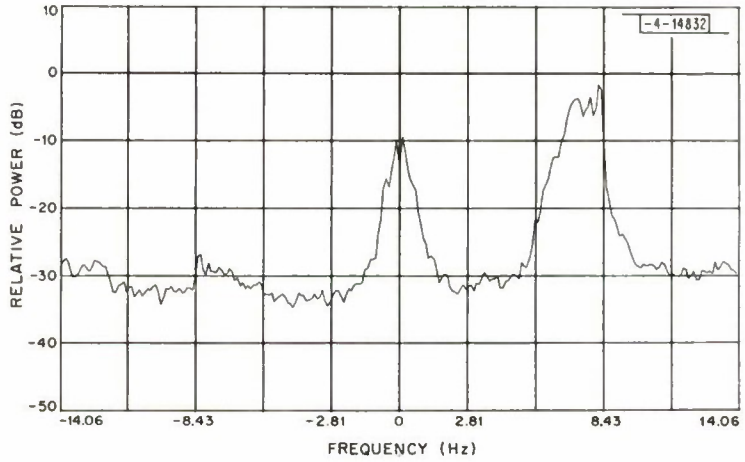

Fig. III-3. Spectrum of transponder in woods inbound. DFT length = 256, sampling rate = 28.12 Hz, resolution = 0.165 Hz, DFTs averaged = 44, target passes = 11, target velocity = 1.35 ft/sec.

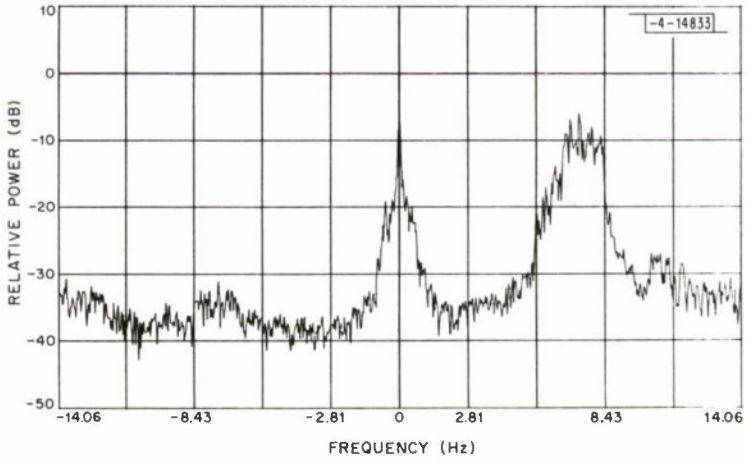

Fig. III-4. Spectrum of transponder in woods inbound. DFT length = 1024, sampling rate = 28.12 Hz, resolution = 0.0412 Hz, DFTs averaged = 11, target passes = 11, target velocity = 1.35 ft/sec.

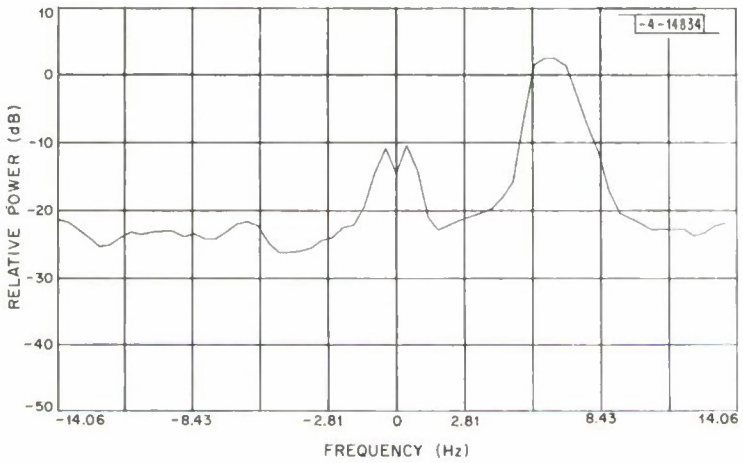

Fig. III-5. Spectrum of transponder in woods outbound. DFT length = 64, sampling rate = 28.12 Hz, resolution = 0.659 Hz, DFTs averaged = 176, target passes = 11, target velocity = 1.35 ft/sec.

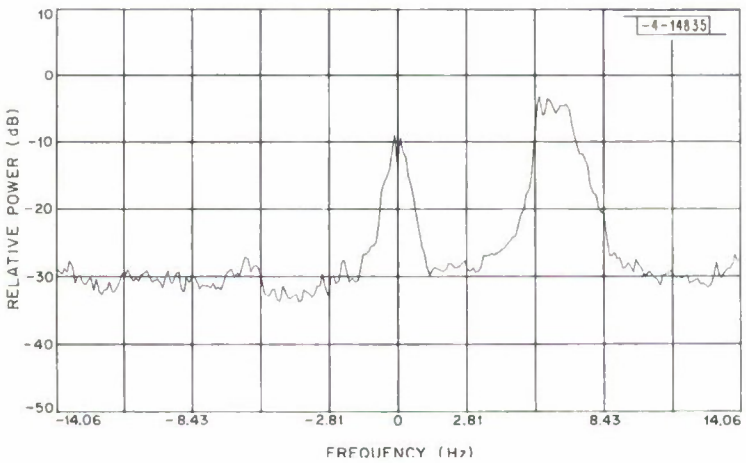

Fig. III-6. Spectrum of transponder in woods outbound. DFT length = 256, sampling rate = 28.12 Hz, resolution = 0.165 Hz, DFTs averaged = 44, target passes = 11, target velocity = 1.35 ft/sec.

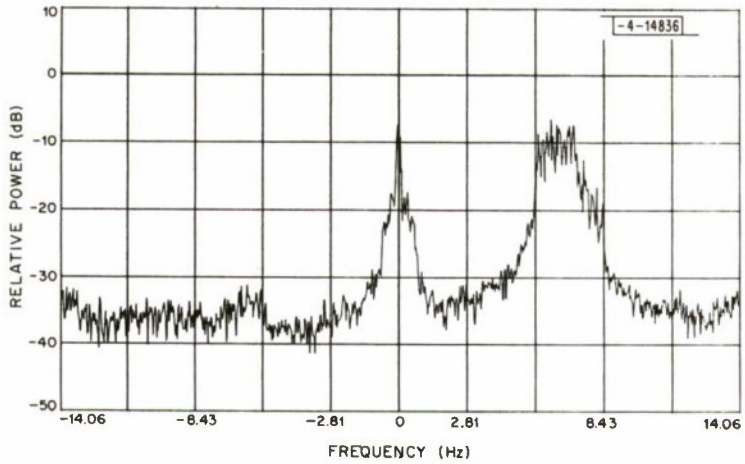

Fig. III-7. Spectrum of transponder in woods outbound. DFT length = 1024, sampling rate = 28.12 Hz, resolution = 0.0412 Hz, DFTs averaged = 11, target passes = 11, target velocity = 1.35 ft/sec.

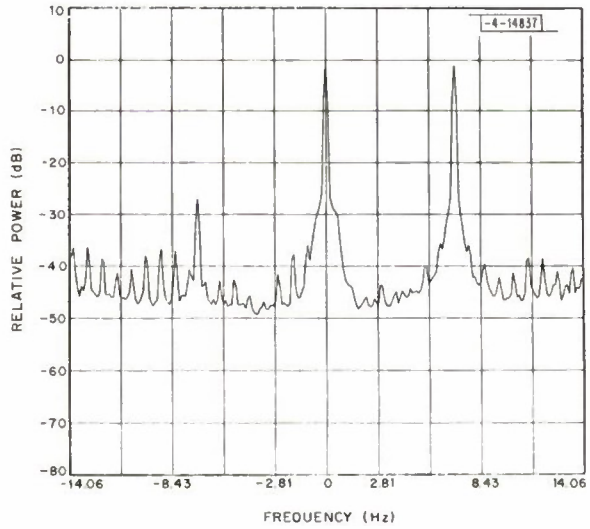

Fig. III-8. Spectrum of transponder at rest in woods with wind. DFT length = 256, sampling rate = 28.12 Hz, resolution = 0.165 Hz, DFTs averaged = 54.

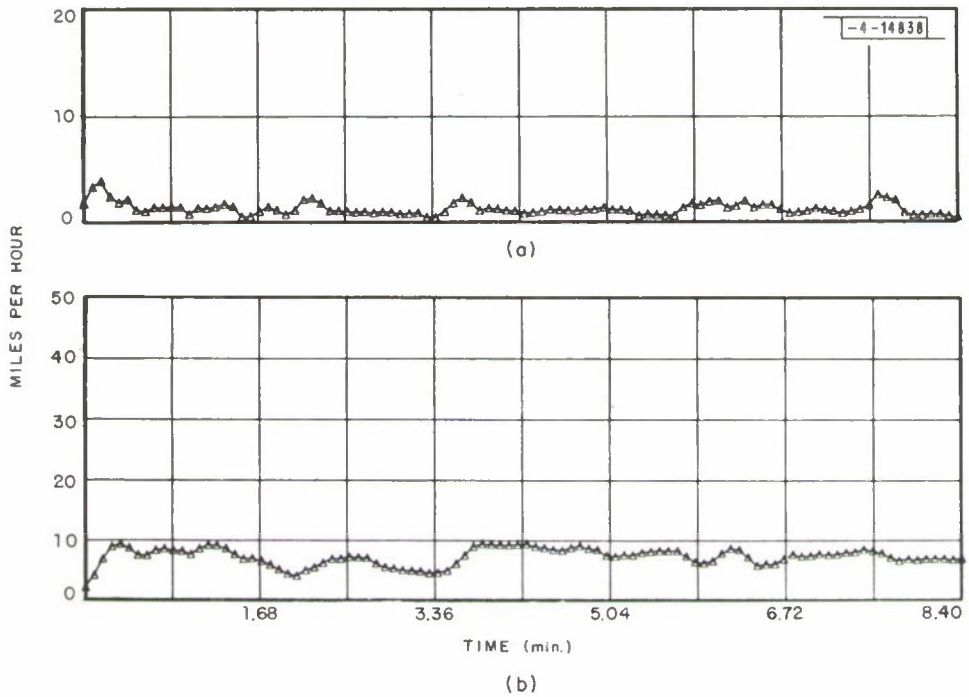

Fig. III-9. Transponder at rest in woods with wind. (a) Running standard deviation of wind; (b) running average of wind.

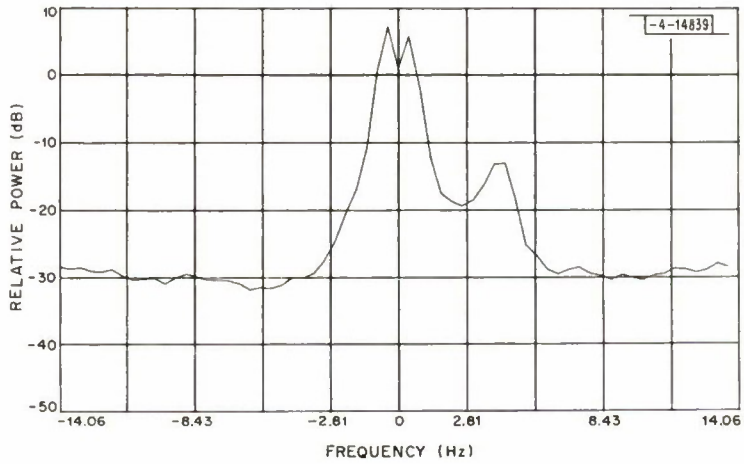

Fig. III-10. Spectrum of man in woods inbound. DFT length = 64, sampling rate = 28.12 Hz, resolution = 0.659 Hz, DFTs averaged = 132, target passes = 11, target velocity = 1.5 m/sec.

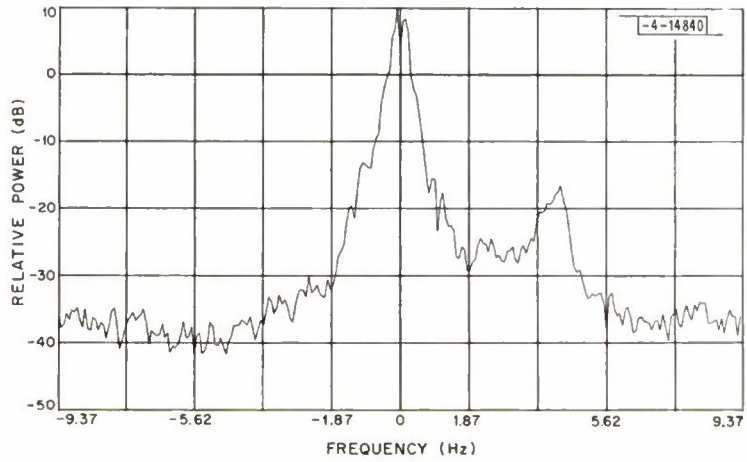

Fig. III-11. Spectrum of man in woods inbound. DFT length = 256, sampling rate = 18.75 Hz, resolution = 0.11 Hz, DFTs averaged = 10, target passes = 10, target velocity = 1.5 m/sec.

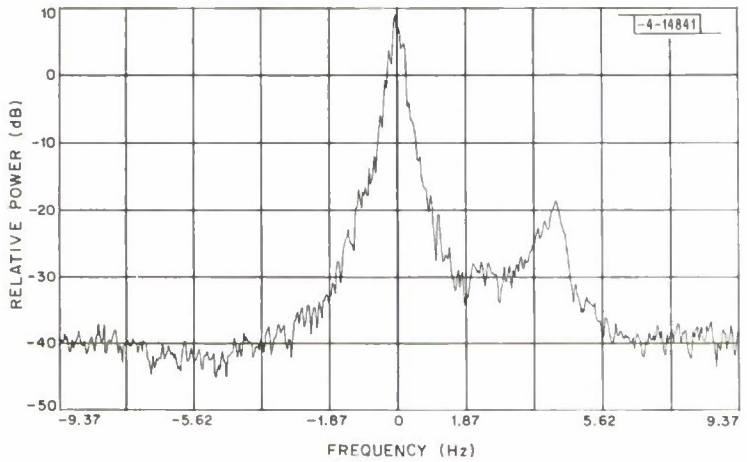

Fig. III-12. Spectrum of man in woods inbound. DFT length = 512, sampling rate = 18.75 Hz, resolution = 0.0549 Hz, DFTs averaged = 10, target passes = 10, target velocity = 1.5 m/sec.

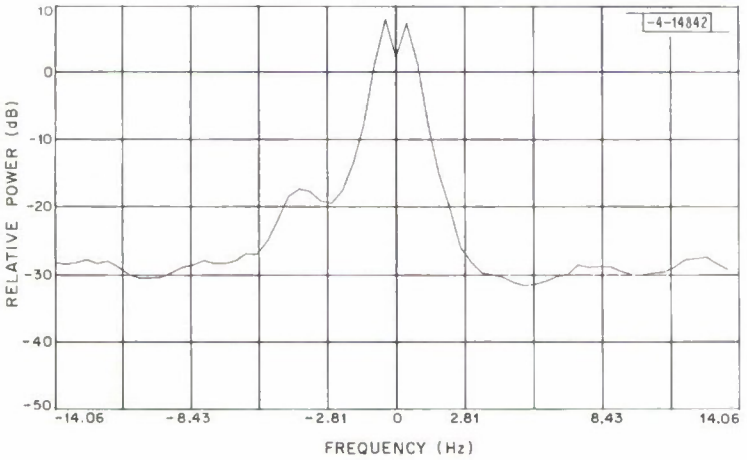

Fig. III-13. Spectrum of man in woods outbound. DFT length = 64, sampling rate = 28.12 Hz, resolution = 0.659 Hz, DFTs averaged = 132, target passes = 11, target velocity = 1.5 m/sec.

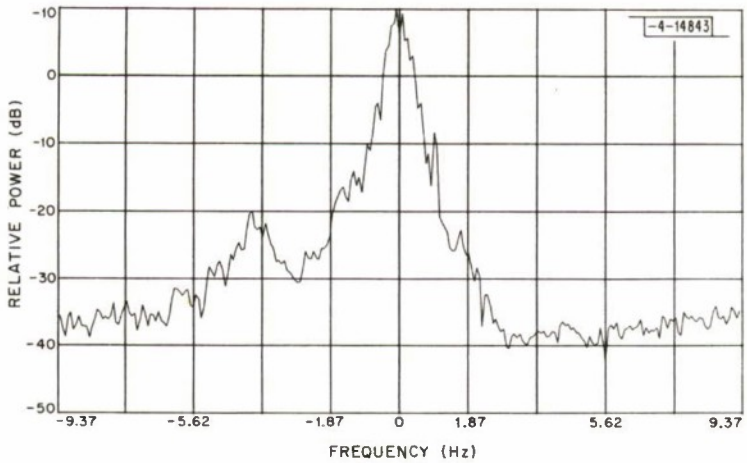

Fig. III-14. Spectrum of man in woods outbound. DFT length = 256, sampling rate = 18.75 Hz, resolution = 0.11 Hz, DFTs averaged = 10, target passes = 10, target velocity = 1.5 m/sec.

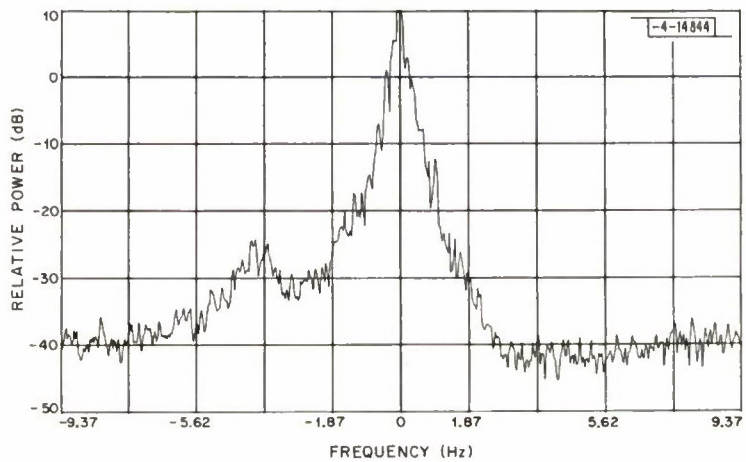

Fig. III-15. Spectrum of man in woods outbound. DFT length = 512, sampling rate = 18.75 Hz, resolution = 0.0549 Hz, DFTs averaged = 10, target passes = 10, target velocity = 1.5 m/sec.

IV. CLUTTER STATISTICS

J. H. Teele
R. D. Yates

A. Theory

In order to design optimum receivers and analyze their performance, the clutter statistics must be known. In Sec. II-A, a clutter model was presented which could predict the clutter spectrum. However, nothing was said about the clutter statistics. If the correlation distances of the random permittivity $\epsilon(\underline{r}, t)$ in the transverse directions are denoted as r_x and r_y, then as long as $r_x \cdot r_y << R \cdot \Delta R \cdot \Delta\theta$, there will be many independent scattering centers in the range-azimuth cell of area $R \cdot \Delta R \cdot \Delta\theta$. Assuming that $\epsilon(\underline{r}, t)$ is homogeneous and isotropic in the transverse directions so that there are no dominant scatterers, one would then postulate that the clutter return is a Gaussian random process.

Consider the clutter return from a single range-azimuth cell as given by Eq. (II-1). It has a power spectral density with an impulse at zero frequency. Hence, the quadrature components contain a DC or specular component and may be expressed as

$$I(t) = G_r^{1/2} [I_o + I_1(t)] \tag{IV-1}$$

$$Q(t) = G_r^{1/2} [Q_o + Q_1(t)] \quad . \tag{IV-2}$$

The random variables I_o and Q_o represent the DC clutter component and are zero mean and uncorrelated with

$$I_o = A \cos\theta \tag{IV-3}$$

$$Q_o = A \sin\theta \tag{IV-4}$$

where θ is a random variable, independent of A, and uniformly distributed between 0 and 2π. The mean square value of the random variable A is the DC clutter power and is given as

$$\begin{aligned} P_{DC} &= E\{A^2\} = E\{I_o^2 + Q_o^2\} \\ &= P_c \cdot R_c(\infty) \quad . \end{aligned} \tag{IV-5}$$

The random processes $I_1(t)$ and $Q_1(t)$ are zero mean, uncorrelated, wide-sense stationary with correlation functions

$$R_{I_1}(\tau) = R_{Q_1}(\tau) = \frac{1}{2} \cdot P_c \cdot [R_c(\tau) - R_c(\infty)] \quad . \tag{IV-6}$$

The AC clutter power is then given as

$$P_{AC} = E\{I_1^2(t) + Q_1^2(t)\} = P_c - P_{DC} \quad . \tag{IV-7}$$

The total clutter power P_c is given by Eq. (II-2), while the normalized clutter correlation function $R_c(\tau)$ is given by Eq. (II-15). In addition, the random variables I_o and Q_o are uncorrelated with the random processes $I_1(t)$ and $Q_1(t)$.

If the clutter can be modeled as a Gaussian random process, then I_o and Q_o are independent Gaussian random variables, A is a Rayleigh random variable, and $I_1(t)$ and $Q_1(t)$ are independent Gaussian random processes.

It should be noted that I_o and Q_o are spatial random variables so that the expectation in Eq. (IV-5) is with respect to the ensemble of possible range cells. The random processes $I_1(t)$ and $Q_1(t)$ evolve in time so that the expectation in Eq. (IV-6) is a temporal one.

Now there are two extensions of the above model which occur in practice. It was assumed that the velocity field was a stationary process in time. A modulation index was defined in Eq. (II-44) as

$$\mu(z) = \frac{4\pi}{\lambda} \cdot \beta(v_o) \cdot z^2 \tag{IV-8}$$

where $\beta(v_o)$ is a monotonically increasing function of the average wind velocity v_o above the trees. Let v_o be slowly varying compared with the AC clutter signals and let it have a correlation time T_o. Then, over a time span T_o, the clutter processes I(t) and Q(t) can be modeled as stationary and Gaussian, conditioned on v_o being known. Over periods much longer than T_o, the clutter probably is not Gaussian and certainly is not statistically stationary.

The second extension concerns the spatial statistics of the clutter. The forest was assumed to be homogeneous and isotropic in the transverse directions. This implies that the clutter area cross section σ_o is constant. Suppose that σ_o is a random process with respect to the transverse directions x, y, and that over the range cell area $R \cdot \Delta R \cdot \Delta\Theta$ it can be considered a constant. Then, conditioned on σ_o being known, the clutter is a Gaussian process. However, over the ensemble of possible range cells, the clutter is not a Gaussian process and its statistics will depend on the statistics of σ_o.

An additional complication is that the two-way clutter propagation factor F_c may also be a function of space due to different free-space forest interface losses, hills, etc.

The spatial statistics of the clutter are important because they indicate the dynamic range needed in the receiver front end.

The type of processing of the time data in a given range-azimuth cell will depend on the temporal clutter statistics. Consider the case of a small phase modulation index. Then, from Eq. (II-22) the clutter power and clutter correlation functions may be written as

$$P_{DC} = P_c \cdot \left(1 - \overline{\mu^2}\right) \tag{IV-9}$$

$$R_{I_1}(\tau) = R_{Q_1}(\tau) = \frac{1}{2} P_{AC} \cdot \rho_D(\tau) \tag{IV-10}$$

$$P_{AC} = P_c \cdot \overline{\mu^2} \tag{IV-11}$$

where $\overline{\mu^2}$ is a mean square modulation index given by the expression

$$\overline{\mu^2} = \left(\frac{4\pi}{\lambda}\right)^2 \int_o^{h_f} W(z)\, z^4\, dz \cdot \beta^2(v_o) \tag{IV-12}$$

and $\rho_D(\tau)$ is the normalized displacement correlation function given by Eq. (II-39).

It is seen that the total clutter power does not depend on the average wind velocity v_o. However, in Sec. II-B it was postulated that $\beta^2(v_o)$ was proportional to v_o^3. Hence, the AC clutter power is very sensitive to the wind velocity. If the Gaussian nature of the clutter is to be deduced from studying the time signal from one range cell, it is important to properly normalize the clutter so that it has a constant mean and variance.

Note that Eqs. (IV-9), (IV-10), and (IV-11) imply that the clutter spectrum shape does not depend on the average wind speed v_o, only the powers do.

B. Experiments

The experiments performed to verify the clutter statistics were limited due to time. No spatial statistics were studied. However, in Ref. 5 it was shown that, for flat, uniform-type foliage, the R^{-7} dependence of the clutter power is correct. The clutter return as a function of range, under the absence of wind, was recorded. A least-squares fit of an R^{-n} dependence of $I^2(R) + Q^2(R)$ was found. Due to recording limitations, the clutter statistics were not studied.

Using the measurement mode of the LRDR, the quadrature components of the clutter from one range cell were recorded for an hour. One quadrature channel was studied and the data reduced to several segments of 8192 points. In each segment, the sampling rate was 11.25 Hz corresponding to a segment duration of 723 sec. A histogram of one of these segments of 8192 points is shown in Fig. IV-1, where it is seen that the probability density is not Gaussian. Similar results were found for other segments.

The data were now filtered to remove the high-energy clutter about zero frequency and the receiver noise. A histogram of the filtered data showed no improvement. For each segment, the 8192 points were divided into B consecutive blocks, with 8192/B points per block. Given a block, the sample mean M and sample variance s^2 were computed and used to normalize the data in the block as follows:

$$\tilde{x}_i = \frac{x_i - M}{s} \tag{IV-13}$$

where x_i are the original data points, and $\tilde{x}_i$ are the normalized data. Histograms were now made for each segment. The case for B = 32 is shown in Fig. IV-2 for the same data used in Fig. IV-1. Each block consisted of 256 points corresponding to a time span of 23 sec. By using the Kalmogorov-Smirnov nonparametric tests,[7] the probability that the 8192 points were independent Gaussian with variance σ^2 and mean m was 50 percent.

Other block lengths were tried since there is a tradeoff between the number of samples needed to estimate the mean and variance, and the time over which the clutter statistics are stationary. It was found that B = 32 gave the highest probability of being Gaussian.

If the N = 8192/B clutter samples in a block were independent identically distributed Gaussian random variables, then $\tilde{x}_i$ as given by Eq. (IV-13) would actually be distributed as $\sqrt{1 - 1/N} \cdot t_{N-1}$, where t_{N-1} has a student-t distribution with N − 1 degrees of freedom. However, for N > 40 there is negligible difference between the t-density and the Gaussian density over the $\pm 3\sigma$ points.

The fact that the histogram in Fig. IV-2 has a greater variance than one obtained from a set of 8192 identically distributed, independent, Gaussian random variables can be caused by the following conditions. The first condition is that the data points are not independent, so that the equivalent degrees of freedom are less than 8192; the second is due to the nonstationary clutter statistics so that the data are not normalized properly.

Based on the above results, it appears that the first-order statistics of the clutter are Gaussian over the correlation time of the average wind velocity above the trees.

However, an extensive study should be made of the temporal statistics of the clutter from several different range cells under different wind conditions. The average wind velocity above the trees in the area studied should be recorded. This will help in correlating wind changes with those in the clutter spectral shape and power, and in properly normalizing the data.

The spatial statistics of the clutter from foliated areas should also be studied. Let $I(R, \Theta, t)$ and $Q(R, \Theta, t)$ be the quadrature components of the clutter from a range-azimuth cell at R, Θ. The quantity

$$\Sigma(R, \Theta) = \frac{\frac{1}{T} \int_0^T [I^2(R, \Theta, t) + Q^2(R, \Theta, t)]\, dt}{P_o \cdot G \cdot A \cdot R \cdot \Delta R \cdot \Delta\Theta} \tag{IV-14}$$

could be computed where T is long enough to smooth out the variations due to wind. The quantities in the denominator are defined in Eqs. (II-2) and (II-3).

If the forest were homogeneous and isotropic over the range-azimuth cells measured, then $\{\Sigma(R_i, \Theta_i)\}$ would be exponentially distributed random variables with a mean value of $\sigma_o F_c$, as given by Eq. (II-7). Hence, a histogram of $\{\Sigma(R_i, \Theta_i) \cdot R_i^8\}$ should be made to see if it is exponential.

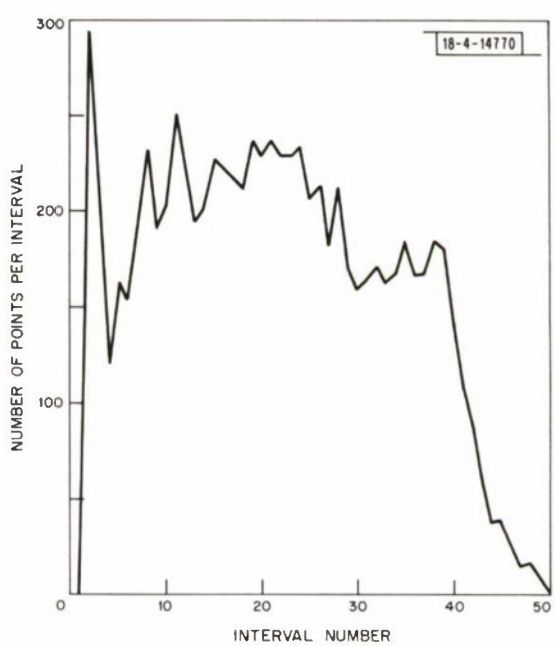

Fig. IV-1. Histogram of unnormalized clutter data.

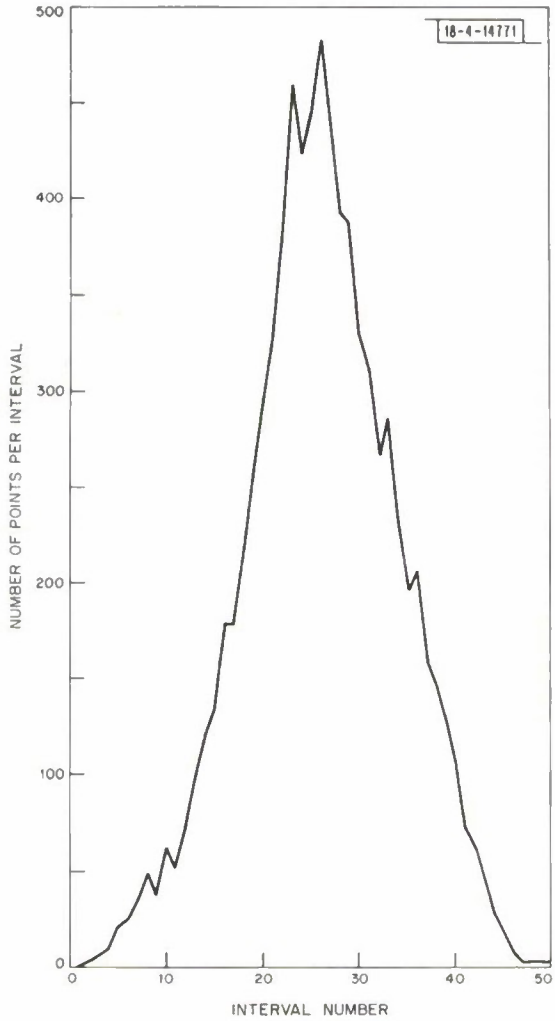

Fig. IV-2. Histogram of normalized clutter data.

V. SUBCLUTTER VISIBILITY IN DIGITAL MTI RADARS

L. Cartledge
R. D. Yates

The purpose of this section is to present an expression for the subclutter visibility in Digital Moving Target Indicating Radars such as the LRDR.

Consider a range-gated, pulse-doppler, MTI radar whose general structure is described by Figs. V-1 and V-2. The transmitted signal consists of an RF pulse which is sent at a fixed prf (pulse repetition frequency). Generally, this pulse will be modulated so that pulse compression can be used to increase the range resolution. For this discussion, it will be assumed that the RF pulse consists of N coherent basic subpulses. A binary code is modulated onto the RF pulse by letting the basic subpulses have an amplitude of ±A. In this manner, the range cell is defined by the basic subpulse provided that the code has a correlation function with low time sidelobes.

The analog section of the receiver is shown in Fig. V-1. The first bandpass filter is used to limit the out-of-band interference. It is followed by a low-noise, wideband, RF amplifier. This amplifier then feeds a variable attenuator, which is followed by a second wideband low-noise RF amplifier, a second bandpass filter, quadrature video detectors, and video amplifiers. In practice, the combination of the second RF amplifier and bandpass filter is implemented with several cascaded wideband RF amplifiers, the bandpass filter being placed in the center of the chain. In a properly designed system, the video noise level is set by the second RF amplifier for most of the attenuator's range.

The digital section of the receiver is shown in Fig. V-2. The in-phase and quadrature video signals are sampled by two analog-to-digital (A/D) converters, followed by a digital transversal filter which performs the pulse compression. The compressed samples are then fed to a digital signal processor which produces a detection statistic for each range-doppler cell to be examined. These statistics then are sent to a thresholding device for decision-making and a display unit.

The digital signal processor may be implemented in several ways. The most flexible is to use a general-purpose, high-speed digital computer which is programmed to compute the detection statistics given the input data. Signal processing algorithms then exist as software packages which can be easily modified. The most inflexible method is to use a hardwired special-purpose computer. Based on the experience gained with the LRDR, the first method should always be used until all the details and operating characteristics of the signal processor are understood. The fixed-point arithmetic and finite word length of the computing machine used can produce quantization and dynamic range problems which can affect the performance of the signal processor in unpredictable ways. In the derivation of the expression for subclutter visibility, it will be assumed that these problems can be neglected.

The dynamic range of the entire system is then limited by the A/D converters and the processing gain following them. The attenuation control must be adjusted as a function of range, for each azimuth, so that the peak signal levels are just below the A/D's maximum input level. In a system where the clutter return is much greater than the target and receiver noise signals, the clutter peaks should not be allowed to saturate the A/Ds. If they do, the clutter spectrum will broaden out, the time sidelobes of the compressed pulse will deteriorate, and a loss in detection performance will result.

Since phase coding is used, the attenuator must be held constant over the basic subpulse duration. As gain changes are made across the received signal, corresponding gain corrections must be introduced in the digital transversal filter so that the pulse compression is correctly performed. The simplest gain change that can be made digitally is a 6-dB change, which corresponds to a word shift. Based on the ground clutter seen with the LRDR, the front-end receiver

gain should not be monotonically increasing with range. One should be able to accommodate clutter hot spots without a loss of subclutter visibility in range cells following the range cell having large clutter.

The second problem that arises with the use of an A/D is the nonlinearity caused by the quantization. Signals whose peak-to-peak excursions are less than a quantizing level can be badly distorted or even lost unless an effective dither device is used. This can be accomplished by injecting receiver noise at the A/D input with an rms value of at least one-half a quantizing level which is independent from sample-to-sample. This is done by making the second bandpass-filter bandwidth equal to the sampling rate of the A/D and by adjusting the gain of the second RF amplifier.

The bandwidth of the second RF amplifier must be greater than or equal to the bandwidth of the basic subpulse transmitted. If it is equal to it, then one has essentially a filter matched to the basic subpulse, and the digital transversal filter consists of $(N - 1)$ shift registers and adders. However, the bandwidth of the second RF amplifier may be greater than that of the basic subpulse, in which case the filter matched to it will be a hybrid filter. If the bandwidth of the filter is twice that of the subpulse then the transversal filter will consist of $2N - 1$ shift registers and adders.

It will be shown that the subclutter visibility can be increased by opening up the bandwidth of the second bandpass filter, adjusting the video noise level, and increasing the A/D sampling rate. However, the receiver eventually will become susceptible to jamming and interference if the bandwidth becomes too great.

In order to derive the optimum receiver structure, a complete statistical description of the clutter, noise, and target signals is necessary. In most cases of interest, the received clutter power is much greater than the target power. Hence, unless their spectra are separated in frequency, reliable detection is impossible due to the limited time-on-target.

It will be assumed that the clutter signal from one range cell can be modeled as a zero mean Gaussian random process whose statistics change slowly compared with the processing time. The process is completely characterized by its power spectral density which is known except for a finite set of parameters. An example would be a spectra of known shape but unknown gain.

The receiver noise can be modeled as a zero mean, band-limited, white Gaussian random process with at most an unknown spectral height. This spectral height will be a function of the gain control which, in turn, will depend on the clutter power. However, for a well-designed system, the noise spectral height will remain constant over most of the operating range of the gain control.

The target returns may be either deterministic or random. For aircraft and ground targets in open areas, where their velocity is constant over the observation time, the target signal can be modeled as a known signal with several unknown parameters. Generally, these would be the amplitude, phase, arrival time, and doppler of the received signal. If a rotating antenna is used, the known form of the signal will depend on the two-way antenna pattern. If a phased array is used in a stepped scan mode, the known signal form will depend on the dwell time and the compressed pulse shape.

The return of a target in foliage will be random. The multipath within the forest causes the field to vary spatially across the range cell which, in turn, modulates the target's return as it passes through the cell. For a constant-velocity target, its spectrum may be expressed as a known function with a finite set of unknown parameters. These parameters could be a gain,

a bandwidth measure, and a frequency shift. It is not clear what the statistics of the target signal are. However, if a great deal of multipath were present, it would seem reasonable to model it as a Gaussian random process with unknown parameters. This process must be time-gated by a pulse which will depend on the compressed pulse and the target's velocity.

In the case of a deterministic signal, the receiver consists of a whitening filter followed by a bank of filters matched to frequency-shifted versions of the target signal that appears at the output of the whitening filter. The matched filters are followed by square law envelope detectors. For an arbitrary observation time, the whitening filter is usually time varying. However, if the observation time is several times the clutter correlation time, the filter becomes time invariant. The output of the whitening filter is white noise when its input is clutter plus receiver noise.

In the case of a random signal which can be modeled as a Gaussian process, the receiver can be implemented in the following manner provided that the observation time is several times the clutter and target correlation time. The receiver consists of a whitening filter followed by a bank of target filters. The outputs of the target filters are square law envelope detected and integrated for the corresponding time-on-target. In general, the target filter will depend on the clutter, receiver noise, and target spectra. However, the target filter has a simple form if over the bandwidth of the target spectrum the target power is appreciably greater than the clutter-plus-noise power. The target filter can then be approximated as having unity gain over this bandwidth, and zero gain elsewhere.

Unless the time-bandwidth product of the target signal is large, in order to obtain reliable detection, the target power must be larger than the clutter-plus-receiver-noise power over the target's bandwidth.

Given a probability of false alarm, the detection probability is directly a function of the receiver's output signal-to-clutter-plus-noise ratio when the signal is deterministic. Unfortunately, for the random signal case, the output signal-to-noise (S/N) ratio cannot be related directly to the detection performance. However, by adding an incoherent integration loss factor, the signal-to-clutter-plus-noise ratio may be used as a criterion for the detection performance. This loss factor will be a function of the target signal's time-bandwidth product, the probability of false alarm, and the probability of detection.

In most cases of interest, the target signal will be competing only with receiver noise once proper filtering has taken place. The clutter return has set the receiver gain level so that the A/Ds are not overloaded. The receiver noise level is set by the linearity requirement of the A/D. Under these assumptions and by using the optimum receiver, the output S/N ratio can be expressed as

$$\left(\frac{S}{N}\right)_o = \left(\frac{S}{C}\right)_i \cdot \frac{G}{L}$$

in which

$\left(\frac{S}{C}\right)_i$ = received peak signal power/received clutter power from compressed range cell

G = processing gain

L = losses .

The processing gain is expressed as follows:

$$G = N \cdot T_{ot} \cdot prf \cdot 2^{2(b-1)} \cdot B_{ad}/B_p$$

in which

N = length of phase code

T_{ot} = time on target

prf = pulse repetition frequency

b = number of bits in A/D

B_{ad} = A/D sampling rate

B_p = bandwidth of compressed pulse.

The loss factor is expressed as

$$L = L_c \cdot L_g \cdot L_{ad} \cdot L_i \quad .$$

The factor L_c represents the loss due to range extended clutter when pulse compression is used. The A/D must accommodate the uncompressed clutter return without limiting. It follows that

L_c = 1 for point clutter

= N for range extended clutter with a uniform cross section over the code duration.

For the most part, the loss L_c will be between 1 and N.

The factor L_g represents the loss due to an increase in the noise level at the A/D as the receiver gain is increased and the front-end noise predominates. For a well-designed system, this will only occur at the maximum range.

The factor L_{ad} represents the loss due to the A/D limiting and linearity margins and is given as

$$L_{ad} = (\delta/\gamma)^2$$

in which

δ = A/D limiting margin. The rms clutter voltage is set to E/δ, where E is the magnitude of the A/D's maximum input.

γ = A/D linearity margin. The rms noise voltage is set to Q/γ, where Q is the A/D's quantizing increment.

The factor L_i represents the incoherent integration loss for random target signals. If the target signal is deterministic, then $L_i = 1$; otherwise,

$$L_i = (T_{ot} \cdot B_s)^{\alpha}$$

in which

T_{ot} = time on target

B_s = target signal bandwidth $\geqslant 1/T_{ot}$.

The factor α is such that $0 \leqslant \alpha \leqslant 1/2$ and is a function of the coherent S/N ratio, probabilities of false alarm and detection, and the time-bandwidth product $T_{ot} \cdot B_s$.

In a forest where the field can be considered a spatially homogeneous random process with a correlation distance of r_c, it follows that the incoherent integration loss can be expressed as

$$L_i = \left(\frac{\Delta R}{r_c}\right)^{\alpha}$$

in which

r_c = correlation distance of the field across the range cell

ΔR = effective range-cell length = $(C/2)\, T_{cell}$, where T_{cell} is the effective compressed pulse duration.

In this case, the target spectrum possesses a constant Q and as the target's velocity increases, its bandwidth increases while the T_{ot} decreases. It has been assumed that the range cell defines the T_{ot} and that the target has a constant velocity.

Given a desired output S/N ratio $(S/N)_{od}$, the subclutter visibility $(S/C)_v$ of a radar with a processing gain G and a loss L can be defined as

$$\left(\frac{S}{C}\right)_v = \left(\frac{S}{N}\right)_{od} \cdot \frac{L}{G} \quad .$$

Then, so long as $(S/C)_i \geqslant (S/C)_v$, the radar will perform adequately.

Given that the clutter area cross section is uniform across the range-azimuth cell, the input signal-to-clutter-power ratio can be expressed as

$$\left(\frac{S}{C}\right)_i = \frac{\sigma_t \cdot F_t}{\sigma_o \cdot F_c \cdot R \cdot \Delta\theta \cdot \Delta R}$$

in which

σ_o = clutter-area cross section

F_c = two-way clutter propagation factor

σ_t = target cross section

F_t = two-way target propagation factor

R = range to range-azimuth cell

$\Delta\theta$ = two-way antenna beamwidth

ΔR = effective range-cell length = $(C/2)\, T_{cell}$

T_{cell} = effective compressed pulse duration.

If all the parameters above are known, it then can be determined whether reliable detections are possible.

In many cases, one would like to compare different radars to determine which performs best. Thus, the comparison should be made on an output S/N ratio basis. Assume that range extended clutter predominates so that $L_c = N$, that the A/D noise level is such that $L_g = 1$, and that the A/D limiting and linearity margins are set so that $L_{ad} = 1$. Then the output S/N power ratio can be expressed as

$$\left(\frac{S}{N}\right)_o = \frac{\sigma_t \cdot F_t}{\sigma_o \cdot F_c} \cdot \frac{T_{ot} \cdot prf}{B_p \cdot (T_{ot} B_s)^{\alpha} \cdot R \cdot \Delta\theta \cdot \Delta R} \cdot B_{ad} \cdot 2^{2(b-1)} \quad .$$

Let us now consider two cases.

Case 1:

Let the dwell time on a range-azimuth cell be long so that the T_{ot} depends on the range-cell length and target velocity. Then, $T_{ot} = \Delta R/V$ where V is the magnitude of the target's radial velocity. For the case of a coherent target signal, it follows that

$$\left(\frac{S}{N}\right)_o = \frac{\sigma_t \cdot F_t}{\sigma_o \cdot F_c} \cdot \frac{prf \cdot T_{cell}}{R \cdot \Delta\Theta \cdot V} \cdot B_{ad} \cdot 2^{2(b-1)} \quad .$$

It should be remembered that $B_{ad} \geqslant 1/T_{cell}$.

In comparing different radar systems, it follows that $(\sigma_t \cdot F_t)/(\sigma_o \cdot F_c)$ is a medium-dependent parameter while the remaining terms are system dependent.

Provided that the target's velocity is constant over the range cell and that the A/D sampling rate remains constant, the output S/N ratio is proportional to the range-cell length. There are system constraints such as noise level and gain adjustments, the RF bandwidth of the receiver, and the complexity of the digital transversal filter that will limit the usefulness of choosing $B_{ad} > 1/T_{cell}$.

If the A/D bandwidth is matched to the compressed pulse bandwidth so that $T_{cell} \cdot B_{ad} = 1$, it then follows that the output S/N power ratio does not depend on the range-cell duration T_{cell}.

There is a tradeoff between the A/D sampling rate and the number of bits, provided that the range-cell duration can be chosen so that $T_{cell} \geqslant 1/B_{ad}$. In this case, a useful figure-of-merit of the A/D can be defined as

$$M = 10 \log_{10} [B_{ad} \cdot 2^{2(b-1)}] \quad .$$

In this manner, different A/Ds may be compared when designing a digital MTI radar.

In the case of a target in foliage where the target return is random, the coherent S/N power ratio must be multiplied by the factor $(\Delta R/r_c)^{-\alpha} = (CT_{cell}/2r_e)^{-\alpha}$. Hence, the output S/N ratio will be proportional to $T_{cell}^{1-\alpha}$. Since $0 \leqslant \alpha \leqslant 1/2$, the system will perform better as T_{cell} is increased, provided that $B_{ad} \geqslant 1/T_{cell}$.

Case 2:

Let the dwell time on the range-azimuth cell be controlled by the antenna scan time and not the target velocity. Then, the output S/N ratio for a coherent target has the following form:

$$\left(\frac{S}{N}\right)_o = \frac{\sigma_t \cdot F_t}{\sigma_o \cdot F_e} \cdot \frac{2 \cdot prf \cdot T_{ot}}{R \cdot \Delta\Theta \cdot C} \cdot B_{ad} \cdot 2^{2(b-1)} \quad .$$

Again it is seen that this expression can be separated into medium and system parameters.

For a fixed A/D sampling rate and provided that $T_{cell} \geqslant 1/B_{ad}$, it is seen that the output S/N power ratio does not depend on the range-cell duration. This property is attained at the expense of the increased digital hardware in the transversal filter. If the A/D sampling rate is matched to the compressed pulse bandwidth, then the output S/N ratio is inversely proportional to the range-cell duration T_{cell}.

As in Case 1, there is a tradeoff between the A/D sampling rate and number of bits. The criterion factor M can be used to compare different A/Ds.

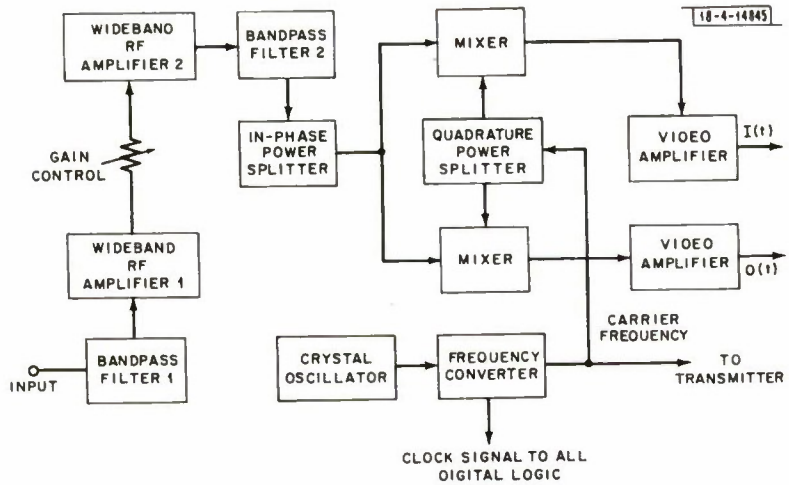

Fig. V-1. Analog section of receiver.

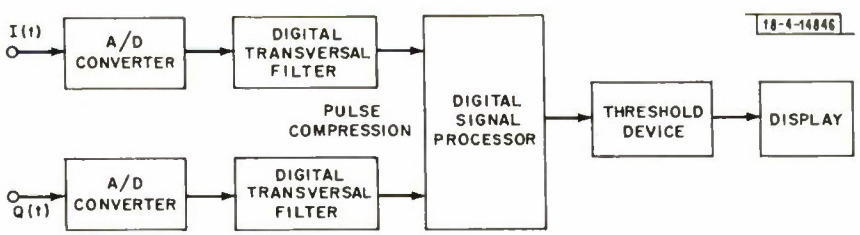

Fig. V-2. Digital section of receiver.

REFERENCES

1. S. Rosenbaum and L. W. Bowles, "Clutter Return from Vegetated Areas," Technical Note 1971-34, Lincoln Laboratory, M. I. T. (10 September 1971), DDC AD-731545.
2. Radar Techniques Program Quarterly Technical Summary, Lincoln Laboratory, M. I. T. (15 November 1971), pp. 8-12, DDC AD-890916-L.
3. D. Middleton, Introduction to Statistical Communication Theory (McGraw-Hill, New York, 1960), pp. 621 and 623.
4. J. L. Lumley and H. A. Panofsky, The Structure of Atmospheric Turbulence, Chapter 5 (Interscience Publishers, New York, 1964).
5. M. Labitt, J. H. Teele and R. D. Yates, "The Lincoln Laboratory Foliage Penetration Radar Measurements Program," see Vol. 1 Bibliography, under Journal Articles.
6. S. Rosenbaum, "Backscatter from a Moving Target in a Randomly Fluctuating Slab (Application to a Vegetated Environment)," Technical Note 1972-2, Lincoln Laboratory, M. I. T. (28 April 1972), DDC AD-744049.
7. F. J. Massey, Jr., "The Kalmogorov-Smirnov Test for Goodness of Fit," Am. Stat. Assoc. J. 46, 68-78 (1951).

DOCUMENT CONTROL DATA – R&D

(Security classification of title, body of abstract and indexing annotation must be entered when the overall report is classified)

1. ORIGINATING ACTIVITY *(Corporate author)* Lincoln Laboratory, M.I.T.	2a. REPORT SECURITY CLASSIFICATION Unclassified 2b. GROUP None

3. REPORT TITLE

An Experimental UHF Ground Surveillance Radar, Volume 2

4. DESCRIPTIVE NOTES *(Type of report and inclusive dates)*

Technical Report

5. AUTHOR(S) *(Last name, first name, initial)*

Cartledge, Lincoln and Yates, Robert D., Editors

6. REPORT DATE 12 October 1972	7a. TOTAL NO. OF PAGES 76	7b. NO. OF REFS 7
8a. CONTRACT OR GRANT NO. F19628-73-C-0002 b. PROJECT NO. ARPA Order 1559 c. 649L d.	9a. ORIGINATOR'S REPORT NUMBER(S) Technical Report 497, Vol. 2 9b. OTHER REPORT NO(S) *(Any other numbers that may be assigned this report)* ESD-TR-72-242	

10. AVAILABILITY/LIMITATION NOTICES

Approved for public release; distribution unlimited.

11. SUPPLEMENTARY NOTES Supplement to ESD-TR-72-241	12. SPONSORING MILITARY ACTIVITY Air Force Systems Command, USAF Advanced Research Projects Agency, Department of Defense

13. ABSTRACT

This is Volume 2 of the final report summarizing two years of work on ground-based foliage-penetration radar. The design and implementation of a breadboard radar system and of a theoretical and experimental investigation of target and propagation phenomena specific to the foliage-penetration problem are described.

Volume 1 comprises three main sections: a short introduction; an overall description of the radar; and detailed descriptions of the hardware and software subsystems in the radar.

Volume 2 describes the use of the radar as a measurements system for studying targets and the clutter environment, in addition to its use for demonstrating the feasibility of radar detection of walking men in foliage. Investigations of target return spectra, clutter return spectra, and clutter return amplitude statistics are reported. Theoretical models relating clutter spectra to wind turbulence and tree resonances are presented and compared with experimental results. Similarly, a previous theoretical prediction of target return spectra is compared with experimental results. Clutter return amplitude statistics are measured and found to be Gaussian under certain conditions. Finally, Vol. 2 contains some comments on the relationships between the subclutter visibility and various parameters of digital MTI systems.

14. KEY WORDS

UHF radar	phased array antenna	radar measurements system
ground surveillance	digital signal processing	digital MTI radar
foliage penetration	ground clutter spectra	target spectra